

POLITECNICO DI TORINO

Master degree course in Electronic Engineering

Master Degree Thesis
in
Photonic Devices

EO Modulators using Plasmonic Waveguides



Supervisor

prof. Giovanni Ghione

Candidate

Claudia MAZZIA 235208

Cosupervisors:

prof. Marco Pirola

prof. Michele Goano

ACADEMIC YEAR 2018 – 2019

To my beloved family

Acknowledgements

Ho tanto di cui ringraziare, non pensavo sarebbe stato così ed invece eccomi qui, alla fine, dopo questo percorso anche troppo lungo, troppo difficile, che mi ha portato gioie e dolori, più dolori forse. Sono pronta a fare quello che per me non è solo un elenco di nomi da ringraziare, sono tasselli della mia vita, sono stati piccole e grandi spinte che mi hanno portato a raggiungere la meta: la mia tanto agognata laurea e libertà.

Come posso non iniziare dalla mia famiglia, quelle persone che per me ci sono sempre e comunque, che mi supportano e mi sopportano (veramente tanto, anche troppo forse), che mi spronano, mi guidano e soprattutto mi vogliono bene nonostante tutto, nonostante non sempre approvino le mie scelte, nonostante mi lamenti veramente tanto, ma che gusto c'è nel fare qualcosa se non ce ne lamentiamo?

Devo ringraziare Roberta meglio nota come Baby per me, anche se penso mi odierà per aver usato questo soprannome in questo contesto. Lei c'è sempre, è lì, non solo quando mi rilasso e lascio emergere il mio lato più piacevole e leggero (nascosto molto in profondità devo ammettere), ma con pazienza ed affetto mi ascolta, anche quando mi lamento e sono abbattuta. Sono fortunata ad averla incontrata.

L'impatto con Torino, con questa nuova vita da fuorisede, con un nuovo ateneo e con le sue regole, è stata una delle cose più dure che io abbia affrontato, non potrò mai smettere di ringraziare abbastanza Vincenzo per il supporto che mi ha dato e la pazienza con cui mi ha trattata anche quando non me la meritavo; Roberta, la mia prima amica qui, il mio faro in un momento in cui non riuscivo a scorgere nessuna luce; Andrea, che mi ha dato un rifugio in un momento in cui avevo un tetto ed un letto dove riposarmi, ma non avevo una casa; Enrico, un caro amico, la persona che è riuscita a darmi un abbraccio, una cosa così semplice eppure così importante, nel momento in cui ne avevo più bisogno, che mi ascolta, mi supporta, mi fa ridere e mi ricorda che la vita non è poi così seria e pesante come in genere mi appare.

Devo ringraziare i miei coinquilini, Martina e Leo, per essere stati la mia piccola famiglia al nord, per i pianti del lunedì, per i pranzi e le cene insieme, per le riunioni sul letto di Martina, per le risate, gli abbracci e gli scherzi. Non mi potevano capitare coinquilini migliori.

Nell'elenco delle persone che mi hanno sopportato non potevo non inserire Eva, quella che considero la mia compagna di tesi anche se non lo eravamo sulla carta, confidente di pensieri, riflessioni, lametele, accomunata dalle mie stesse paure e per questo forse una delle persone che mi potevano capire di più.

Ultima, ma non ultima, quella che è stata prima mia collega, ma che è diventata una tra le persone più importanti per me, Sonia, una delle mie migliori amiche, compagna di scleri e di cibo, non importa quanto siamo lontane, non ci perdiamo e continuiamo a sostenerci nonostante il nostro pessimismo cosmico.

Summary

Optical modulators are key components in the design of high speed optical communication systems. In particular, Electro-Optic Mach Zehnder modulators (EO MZM) realized in LiNbO_3 are a well established and reliable solution in long haul communication, suitable to encode both analog and digital information. Even though the operating principle is the linear electro-optic effect (Pockels Effect), these devices are considered interferometers since they exploit the interference between two phase shifted light beams to obtain an amplitude modulation. The appealing feature of LiNbO_3 MZM is the possibility to obtain a good trade off between the need to have low losses, low driving voltages, broad bandwidth and low chirp, while a big drawback is the large footprint ($\sim \text{cm}^2$) that poses a severe limitation when compact and performing devices are needed [7]. In the search of a valid alternative to LiNbO_3 MZM, when very small dimensions are required, Plasmonic POH Modulators emerged as promising devices ideally capable of providing a large bandwidth ($>100\text{GHz}$), small energy consumption ($\sim 25\text{fJ/b}$) and a very small voltage-length product ($\sim 40\text{V}\mu\text{m}$) with a footprint of the order of few μm^2 . In these structures, Metal-Insulator-Metal (MIM) waveguides are integrated on SOI wafer; light propagates as surface plasmons at the metal-insulator interfaces making possible to achieve sub-wavelength field confinement which is main cause of the small dimensions. In this thesis work a study of a Plasmonic Mach-Zehnder modulators is proposed. Starting from the analysis of the basic Electro-Optic Mach Zehnder modulator structure, a block model developed in a microwave CAD environment is proposed, it gives the possibility to design and optimize the driver and modulator within the same circuit environment[5]. The last part focuses on the description of wave propagation through plasmonic structures and shows some simulation results obtained integrating the electric characteristics of plasmonic structures in the block model previously described.

Contents

List of Figures	9
1 EO Mach-Zehnder modulator: Theoretical Introduction	11
1.1 Introduction	11
1.2 Lumped Case	12
1.2.1 System Level Description	12
1.3 Distributed Case	18
1.3.1 Co-propagating RF and optical waves	19
1.3.2 Counter-propagating RF and optical waves	21
1.3.3 Frequency Response	24
1.4 Chirp Model	27
2 EO Mach-Zehnder modulator: Multi-Sectional Model	31
2.1 Introduction	31
2.2 Modelling	32
2.3 Phase-Modulation Block	33
2.3.1 Mathematical Formulation	34
2.3.2 Modelling	37
2.4 AM Block	40
2.5 Implementation	41
2.5.1 Phase Modulator Implementation	42
2.5.2 Interferometer Implementation	43
3 Plasmonic Waveguides	45
3.1 Introduction	45
3.2 Characterization	46
3.2.1 Oscillatory Modes	51
3.3 Metal-Dielectric Interface	52
3.4 Metal-Dielectric-Metal waveguide	54
3.4.1 Lossless Media	55

4 EO Plasmonic Mach-Zehnder modulator	65
4.1 Introduction	65
4.2 POH Modulator	66
4.3 Implementation Details	67
Bibliography	81

List of Figures

1.1	[2] Mach-Zehnder Modulator.	12
1.2	[2] Co-propagating Circuit Schematic.	19
1.3	Counter-propagating Circuit Schematic.	22
1.4	Counter-propagating Circuit Schematic.	23
2.1	[5] Schematic of a Mach-Zehnder Amplitude Modulator.	33
2.2	[3] Phase-Modulation Block.	34
2.3	[3] Optical Phase Line.	39
2.4	[3] Interferometer.	40
3.1	[6] Plasmonic Waveguide.	46
3.2	[6] Metal Dielectric Structure.	52
3.3	Field Components for TM modes.	53
3.4	[6] Field Components for TM modes.	55
3.5	$H_y(x)$ field component for the propagating modes.	60
3.6	effective index for the oscillatory TE and TM modes	63
3.7	effective index TM_0 and TM_1 plasmonic and modes and for the TM_1 oscillatory one.	63
4.1	[7] Plasmonic Mach-Zehnder Modulator.	66
4.2	RF Effective Refractive Index, Loss, Real and Imaginary Character- istic Impedance.	68
4.3	[9] Plasmonic Mach-Zehnder Modulator: reference structure.	69
4.4	Real and Imaginary Permittivity of Gold.	70
4.5	Dielectric Permittivity of SiO_2	71
4.6	Circuit Schematic.	72
4.7	Output Phase Shift.	73
4.8	Small Signal Circuit Schematic.	74
4.9	Small Signal Response.	75
4.10	Frequency Response.	76
4.11	Small Signal Response: anomaly.	77
4.12	Circuit Schematic for Distortion.	78
4.13	Input Signals.	79
4.14	Distortion.	79

Chapter 1

EO Mach-Zehnder modulator: Theoretical Introduction

1.1 Introduction

An overview on the basic principles of the Electro-Optical Mach Zehnder modulator is presented in this chapter.

This device performs an amplitude modulation through the recombination of two phase-modulated beams, the input light is injected into an beam splitter, the resulting beams propagate in the two arms and experience a variation of their phase due to the linear EO effect (Pockel's Effect) or other effects leading to the modulation of the refractive index, such as the Kerr effect or the plasma effect. When a voltage is applied at the central electrode, the resulting electric field in the transverse direction of the arm provides a refractive index variation and so a phase variation. The two beams are recombined at the output with a certain ratio by a beam combiner. The analysis starts from the lumped case characterizing the overall structure and

its behaviour, then the travelling wave case is analysed considering the transmission line theory applied to this specific case, the chirp model is finally described from the result obtained in the lumped case.

1.2 Lumped Case

[2][3] In this section a description of the MZ-model is provided when the device can be seen as lumped element, characterizing its behaviour through its fundamental parameters, then the DC amplitude analysis and the small-signal one are discussed.

1.2.1 System Level Description

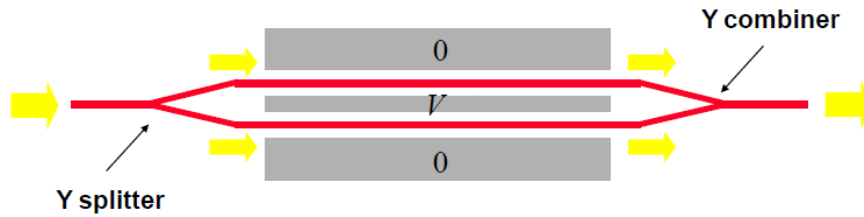


Figure 1.1. [2] Mach-Zehnder Modulator.

A MZ-EO Modulator consist of the cascade of three sections:

- a first beam splitter region which is an Y-junction splitter;
- a modulation section made of two optical waveguides (arms of the modulator), lying between three electrodes;
- the last region is an optical beam combiner (Y-junction beam combiner).

The working principle exploited to obtain the shifting of the beam phases is the electro-optic effect, in this particular case the Pockels Effect (i.e. linear electro-optical effect) is considered in crystals like LiNbO_3 or in organic electro-optic polymers.

Even though the physical modulating effect exploited is a phase modulation, the total modulation at the output comes from the interference between two optical phase-modulated beams (i.e. at the output an amplitude modulation is exploited),

that is why they are considered interferometric devices. Considering a single arm, the variation of the refractive index is proportional to the applied voltage as follows:

$$\Delta n = aV = -\frac{n_e^3 r_{33} V}{2G} \Gamma_{m0} \quad (1.1)$$

defining

$$a = -\frac{n_e^3 r_{33}}{2G} \Gamma_{m0}$$

where G is the distance between the signal electrode and the ground plane, r_{33} is the electro-optic linear tensor element, n_e is the material extraordinary refractive index, and Γ_{m0} is the overlap integral between the optical E_{op} and electrical E_z field expressed as follows:

$$\Gamma_{m0} = \frac{G \iint \|E_{op}(r)\|^2 E_z(r) dS}{V \iint E_{op}(r) dS}$$

where λ_0 is the working wavelength. The phase difference induced by the applied voltage is evaluated integrating the variation of the refractive index over the length of the arm

$$\Delta\Phi = \frac{2\pi}{\lambda_0} \int_0^L \Delta n dx = -\frac{2\pi n_e^3 r_{33} V L}{\lambda_0 2G} \Gamma_{m0} = -\frac{2\pi}{\lambda_0} a L V. \quad (1.2)$$

In the overall structure, the two arms are driven by voltages equal in magnitude but opposite in sign since the RF signal is applied at the centre electrode while the external electrodes are grounded. Generally the two $\Delta\Phi$ are opposite but they will be denoted with the subscript U and L (referring respectively for the upper and lower arm) since in some cases the overlap integral, and so the proportionality factor a , are not the same in the two arms, it happens for example in Z-cut MZ lithium niobate Modulators. Therefore the expressions of the induced phase shift in the two arms are:

$$\Delta\Phi_U = -\frac{2\pi}{\lambda_0} a_U L V$$

$$\Delta\Phi_L = \frac{2\pi}{\lambda_0} a_L L V.$$

The *ON-OFF* behaviour of the modulator depends on the total induced phase-shift i.e. on the difference between the upper and lower phase shift at the output

$$\Delta\Phi_U - \Delta\Phi_L = -\frac{2\pi}{\lambda_0} (a_U - a_L) L V.$$

In the symmetric case $a_U = a_L = a$, the expression becomes:

$$\Delta\Phi_U - \Delta\Phi_L = -\frac{4\pi}{\lambda_0}aLV.$$

The device is *ON* when the phase difference $\Delta\Phi_U - \Delta\Phi_L$ is zero (constructive interference) and so $V = 0$, in this case the optical beam experiences a constructive interference and the characteristic mode is excited at the output; the device is in the *OFF-state* when the phase difference is equal to π , the interference is destructive and only the radiating modes can be found at the output. In the *OFF-state* we obtain:

$$\Delta\Phi_U - \Delta\Phi_L = -\frac{4\pi}{\lambda_0}aLV_\pi = \pi. \quad (1.3)$$

When the modulator is symmetric $\Delta\Phi_U = \Delta\Phi_L = \pi/2$, instead, in the non symmetric case, the two induced phase shifts have different values but their sum has to be π .

From (1.3), it is possible to find the *ON- OFF* voltage V_π ,

$$V_\pi = \frac{\lambda_0}{2|a_U + a_L|L}$$

while in the symmetric case

$$V_\pi = \frac{\lambda_0}{2|a|L}.$$

DC EO Amplitude Response

Another significant parameter to describe the behaviour of the MZ Modulator is $T(V_{in})$ the ration between the power injected P_{in} and the power transmitted at the output P_{out} .

The beam is injected in an input splitter described electrically considering its scattering matrix. Considering the input port (port 1) matched, the two output ports (port 2 and 3) isolated and supposing negligible losses ($\mathbf{S}_{sp}\mathbf{S}_{sp}^T = 1$), the Y-junction S-matrix is expressed as follows:

$$S_{sp} = \begin{pmatrix} 0 & \sqrt{\alpha}e^{j\phi_{sp}} & \sqrt{1-\alpha}e^{j\phi_{sp}} \\ \sqrt{\alpha}e^{j\phi_{sp}} & 0 & 0 \\ \sqrt{1-\alpha}e^{j\phi_{sp}} & 0 & 0 \end{pmatrix}$$

where α is a factor representing the asymmetry in the power splitting of the Y-junction (in presence of symmetric splitters $\alpha = 1/2$). From the Scattering Matrix it is possible to estimate the two output power waves b_2 and b_3

$$S_{ij} = \left. \frac{b_i}{a_j} \right|_{a_k=0 \forall k \neq j},$$

$$b_2 = \sqrt{\alpha} e^{j\phi_{sp}} a_1,$$

$$b_3 = \sqrt{1 - \alpha} e^{j\phi_{sp}} a_1$$

defining a_1 as the incident optical power wave at port 1.

The splitted beams experience a phase delay due to the propagation through the two modulator arms described by \mathbf{S}_{arms}

$$\mathbf{S}_{arms} = \begin{pmatrix} 0 & e^{-jk_0L} \\ e^{-jk_0L} & 0 \end{pmatrix}$$

Therefore the power waves at the combiner upper and lower inputs are:

$$a'_2 = \sqrt{\alpha} e^{j\phi_{sp}} a_1 e^{-jk_0L - j\Delta\Phi_U}$$

$$a'_3 = \sqrt{1 - \alpha} e^{j\phi_{sp}} a_1 e^{-jk_0L - j\Delta\Phi_L}.$$

The output beam combiner is described by a scattering matrix $\mathbf{S}_c \equiv \mathbf{S}_{sp}$ and so the optical power wave at the output (b'_1) is:

$$b'_1 = e^{2j\phi_{sp}} e^{-jk_0L} \left[\alpha e^{-j\Delta\Phi_U} + (1 - \alpha) e^{-j\Delta\Phi_L} a_1 \right]. \quad (1.4)$$

Supposing that the input and output optical waveguides have the same characteristic impedance, it is possible to estimate the ratio between the optical input and output power $T(V_{in})$ as follows:

$$T(V_{in}) = \frac{P_{out}}{P_{in}} = \left| \frac{b'_1}{a_1} \right|^2 = \eta \{ 1 + 2\alpha(1 - \alpha) [\cos(\Delta\Phi_U - \Delta\Phi_L) - 1] \} \quad (1.5)$$

where

$$\eta \approx e^{-\alpha_0 L - A_{sp} - A_c}$$

is a factor that represents the optical insertion loss of the lower and upper arms, in this case it is supposed to be voltage independent; α_0 is the optical loss of the modulator waveguides, A_{sp} is the loss factor of the splitter and A_c is the loss factor of the combiner. Considering symmetrical splitter and combiner (i.e. $\alpha_0 = 1/2$) but with asymmetrical upper and lower branches, equation (1.5) becomes

$$T(V_{in}) = \frac{\eta}{2} [1 + \cos(\Delta\Phi_U - \Delta\Phi_L)].$$

In order to evaluate the static transfer curve, $T(V_{in})$ has to be expressed as function of the time domain voltages v_{inU} and v_{inL} respectively applied at the upper and lower arms. Starting from the induced phase shifts in the two arms

$$\Delta\Phi_U = \pi \frac{v_{inU}}{V_{\pi U}}, \quad \Delta\Phi_L = \pi \frac{v_{inL}}{V_{\pi L}}, \quad (1.6)$$

the *ON – OFF* voltages of the two branches can be obtained as follows

$$|\Delta\Phi_{U,L}| = \frac{2\pi}{\lambda_0} |a_{U,L}| = \pi$$

$$V_{\pi U,L} = \frac{\lambda_0}{2|a_{U,L}|} L.$$

Finally, it is possible to evaluate $T(v_{in})$

$$T(v_{in}) = \frac{\eta}{2} \left\{ 1 + \cos \left[\pi \left(\frac{1}{V_{\pi U}} + \frac{1}{V_{\pi L}} \right) v_{in} \right] \right\} = \frac{\eta}{2} \left\{ 1 + \cos \left(\pi \frac{v_{in}}{V_{\pi}} \right) \right\}$$

where $v_{inU} = v_{inL} = v_{in}$ and V_{π} (modulator *ON – OFF* voltage) is defined as follows

$$V_{\pi} = \frac{V_{\pi U} V_{\pi L}}{V_{\pi U} + V_{\pi L}}.$$

Small Signal Analysis

The small signal operations are performed with respect to a DC working point, in this case the analysis is performed around $V_{\pi}/2$ since it is the optimum point for linearity.

$$v(t) = V_{DC} + \hat{v}(t), \quad v_{in}(t) = V_{in,DC} + \hat{v}_{in}(t)$$

where $v(t)$ is the time-varying open circuit voltage of the real generator connected to the modulator, $v_{in}(t)$ is the input voltage expressed as a function of $v(t)$ including R_G (generator resistance of the input equivalent circuit) and C_{in} (modulator input capacitance).

Linearizing around the bias point, the normalized output power is obtained as:

$$\begin{aligned} \frac{p_{out}(t)}{P_{in}} &= \frac{\eta}{2} \left\{ 1 + \cos \left(\pi \frac{V_{in,DC} + \hat{v}_{in}(t)}{V_{\pi}} \right) \right\} \approx \\ &\approx \frac{\eta}{2} \left\{ 1 + \cos \left(\pi \frac{V_{in,DC}}{V_{\pi}} \right) \right\} - \eta \frac{\pi}{2V_{\pi}} \left\{ 1 + \cos \left(\pi \frac{V_{in,DC}}{V_{\pi}} \right) \hat{v}_{in}(t) \right\} \end{aligned}$$

which can be also written as:

$$\frac{p_{out}(t)}{P_{in}} = \frac{P_{out,DC}}{P_{in}} - \frac{\hat{p}_{out}(t)}{P_{in}}$$

At $V_{in,DC} = V_{\pi}/2$ the previous equation becomes

$$\frac{p_{out}(t)}{P_{in}} \approx \frac{\eta}{2} - \eta \frac{\pi}{2} \frac{\hat{v}_{in}(t)}{V_{\pi}}.$$

Moving on to the frequency domain, the normalized output power $\hat{p}_{out}(t)/P_{in}$ becomes:

$$\frac{\hat{P}_{out}(\omega)}{P_{in}} = \eta \frac{\pi}{2} \frac{V_{in}(\omega)}{V_{\pi}} = \eta \frac{\pi}{2} H(\omega) \frac{V(\omega)}{V_{\pi}} \quad (1.7)$$

where the relationship between the input voltage phasor $V_{in}(\omega)$ and the generator voltage phasor $V(\omega)$ is represented by a low-pass transfer function $H(\omega)$ as follows

$$V_{in}(\omega) = H(\omega)V(\omega).$$

From (1.7) and considering that $|H(0)| = 1$, it is possible to evaluate the modulator frequency response $m(\omega)$ as:

$$m(\omega) = \frac{|\hat{P}_{out}(\omega)|}{|\hat{P}_{out}(0)|} = |H(\omega)|. \quad (1.8)$$

Recalling that the modulator is composed of two sections: a linear and dispersive system (phase modulation section) and a non-linear memoryless one (combiner), it can be demonstrated[1] that the overall normalized frequency response coincides with phase modulation section frequency response. Supposing that (1.6) holds for time-varying input voltages, the phase delays associated to the upper and lower arms are:

$$\Delta\Phi_U = \pi \frac{V_{in}(\omega)}{V_{\pi}U} = \pi H(\omega) \frac{V(\omega)}{V_{\pi}U}$$

$$\Delta\Phi_L = -\pi \frac{V_{in}(\omega)}{V_{\pi}L} = -\pi H(\omega) \frac{V(\omega)}{V_{\pi}L}$$

formulated assuming that the same voltages have been applied to the upper and lower arms. The frequency response is obtained as follows:

$$\frac{\Delta\Phi_{\alpha}(\omega)}{\Delta\Phi_{\alpha}(0)} = H(\omega), \alpha = U, L.$$

The modulator transfer function considering an input capacitance C_{in} and the generator resistance R_G is evaluated from :

$$V_{in}(\omega) = V(\omega) \frac{1}{1 + j\omega C_{in}R_G} = H(\omega)V(\omega). \quad (1.9)$$

The modulator response is obtained substituting the expression of $H(\omega)$ in (1.8)

$$m(\omega) = |H(\omega)| = \frac{1}{\sqrt{1 + \omega^2 R_G^2 C_{in}^2}}. \quad (1.10)$$

To find the 3dB electrical bandwidth

$$m(f_{3dB,el})|_{dB} = -3dB$$

substituting 1.10

$$m(f_{3dB,el})|_{dB} = 20 \log_{10}[m(f_{3dB,el})] = 20 \log_{10} \frac{1}{\sqrt{1 + \omega^2 R_G^2 C_{in}^2}} = -3dB$$

$$2\pi f_{3dB,el} R_G C_{in} = 1$$

$$f_{3dB,el} = \frac{1}{2\pi R_G C_{in}}.$$

Similarly, for the evaluation of the 3dB optical bandwidth

$$m(f_{3dB,op})|_{dB} = -3dB.$$

Since

$$m(f_{3dB,el})|_{dB} = 2m(f_{3dB,op})|_{dB},$$

the resulting $f_{3dB,op}$ is:

$$f_{3dB,op} = \sqrt{3} f_{3dB,el} = \frac{\sqrt{3}}{2\pi R_G C_{in}}.$$

1.3 Distributed Case

[2][3] This section focuses on the description of a uniform Travelling Wave MZ EO Modulator. A closed form model for the optical response of the modulator is obtained through the study of the distributed interaction between the RF and optical field both in the co-propagating and counter-propagating case, supposing that the active area (i.e. the region where the interaction between the optical and electrical fields takes place) is described as a uniform transmission line terminated by a generator and a load at the ends.

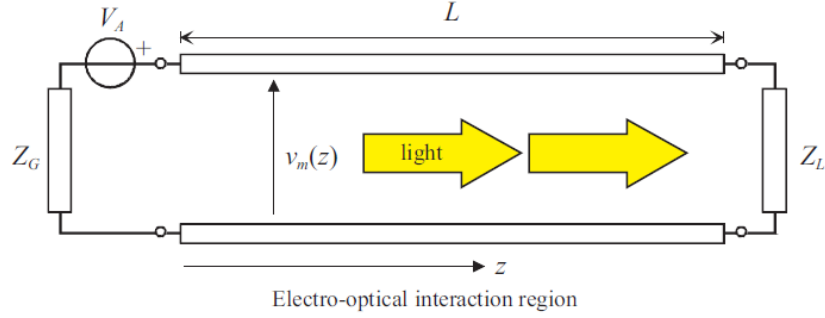


Figure 1.2. [2]Co-propagating Circuit Schematic.

1.3.1 Co-propagating RF and optical waves

The following analysis is performed taking as reference the circuit in Fig.1.2 and supposing the optical and RF signals travelling in the same direction.

To evaluate the variation of the refractive index it is necessary to know the RF voltage applied at each arm. Starting from the input impedance Z_{in} , it is possible to estimate the input voltage at the beginning of the transmission line V_{in}

$$Z_{in} = Z_0 \frac{Z_L + Z_0 \tanh(\gamma_m L)}{Z_0 + Z_L \tanh(\gamma_m L)}$$

where Z_0 is the characteristic impedance of the line, Z_L is the load impedance and γ_m is the RF signal propagation constant in the metal electrode. It is defined as:

$$\gamma_m = \alpha_m + j\beta_m$$

with α_m representing the line losses and $\beta_m = \frac{\omega}{c} n_m$ (n_m is the microwave refractive index). Therefore V_{in} is obtained as follows:

$$V_{in} = E_G \frac{Z_{in}}{Z_g + Z_{in}}.$$

The total input voltage can be expressed as the superposition of a progressive (V_{in}^+) and a regressive i.e. reflected (V_{in}^-) component.

$$V_{in} = V_{in}^+ + V_{in}^- = V_{in}^+(1 + \Gamma_{in}) \quad (1.11)$$

where

$$\Gamma_{in} = \frac{Z_L - Z_0}{Z_L + Z_0} e^{-2\gamma_m L} \quad (1.12)$$

From (1.11) and (1.12) it is possible to find an expression of the progressive and regressive input voltages

$$\begin{cases} V_{in}^+ = V_{in} \frac{(Z_L + Z_0)e^{\gamma_m L}}{(Z_L + Z_0)e^{\gamma_m L} + (Z_L - Z_0)e^{-\gamma_m L}} \\ V_{in}^- = V_{in} \frac{(Z_L - Z_0)e^{-\gamma_m L}}{(Z_L + Z_0)e^{\gamma_m L} + (Z_L - Z_0)e^{-\gamma_m L}} \end{cases} \quad (1.13)$$

Remembering that the voltage in a generic point of a transmission line is given by

$$V(z) = V_{in}^+ e^{-\gamma_m z} + V_{in}^- e^{\gamma_m z}$$

and substituting (1.13), the result is:

$$V(z) = E_G \frac{Z_{in}}{Z_g + Z_{in}} \frac{(Z_L + Z_0)e^{\gamma_m(L-z)} + (Z_L - Z_0)e^{-\gamma_m(L-z)}}{(Z_L + Z_0)e^{\gamma_m L} + (Z_L - Z_0)e^{-\gamma_m L}}.$$

In the time domain

$$V(z, t) = E_G \frac{Z_{in}}{Z_g + Z_{in}} \frac{(Z_L + Z_0)e^{\gamma_m(L-z)} + (Z_L - Z_0)e^{-\gamma_m(L-z)}}{(Z_L + Z_0)e^{\gamma_m L} + (Z_L - Z_0)e^{-\gamma_m L}} e^{j\omega t} = V(z) e^{j\omega t}$$

where ω is the microwave field angular frequency and $V(z)$ is the phasor associated to the RF voltage.

An optical beam with field group velocity v_0 is supposed to enter the active region at $z = 0$ and $t = t_0$, the expression of the resulting voltage $v_m(z, t(z))$ applied at a generic position z of the active region ($0 \leq z \leq L$ with L total length of the active area) at the time $t(z) = t_0 + z/v_0$ is

$$v_m(z, t(z)) = V\left(z, t_0 + \frac{z}{v_0}\right) = V(z) e^{j\omega\left(t_0 + \frac{z}{v_0}\right)} = V(z) e^{j\omega t} e^{j\beta_o z}$$

where

$$\beta_o = \frac{\omega}{v_0} = \frac{\omega n_o}{c_0}$$

is the equivalent propagation constant of the guided mode supposing the optical losses negligible. The local change of refractive index due to an applied RF voltage results in a variation of β_o :

$$\Delta\beta = \frac{\pi}{\lambda_0} \frac{n^3 r \Gamma}{G} v_m(z). \quad (1.14)$$

It is possible to evaluate the induced phase shift $\Delta\Phi_{co}$ integrating $\Delta\beta$ over $[0, L]$. At time $t = t_0$ it is given by

$$\Delta\Phi_{co}(f, t_0) = \int_0^L \Delta\beta dz = \frac{\pi}{\lambda_0} \frac{n^3 r \Gamma}{G} E_G \frac{Z_{in}}{Z_i n + Z_G} \cdot \int_0^L \frac{(Z_L + Z_0)e^{\gamma_m(L-z)} + (Z_L - Z_0)e^{-\gamma_m(L-z)}}{(Z_L + Z_0)e^{\gamma_m L} + (Z_L - Z_0)e^{-\gamma_m L}} e^{j\omega t_0} e^{j\beta_0 z} dz.$$

Defining

$$F(u_{\pm}) = \frac{1 - u_{\pm}}{u_{\pm}}$$

where

$$u_{\pm} = (\pm\gamma_m - j\beta_0)L = j(\pm\beta_m - \beta_0)L \pm \alpha_m L = \pm\alpha_m L + j\frac{\omega}{c_0}(\pm n_m - n_o)L.$$

It is possible to define the total phase shift as

$$\Delta\Phi_{co}(f, t_0) = \frac{\pi}{\lambda_0} \frac{n^3 r \Gamma L}{G} E_G \frac{Z_{in}}{Z_{in} + Z_G} \frac{(Z_L + Z_0)F(u_+) + (Z_L - Z_0)F(u_-)}{(Z_L + Z_0)e^{u_+} + (Z_L - Z_0)e^{u_-}} e^{j\omega t_0}.$$

1.3.2 Counter-propagating RF and optical waves

In the case of RF and optical signals propagating in opposite directions, two different scenarios are possible concerning the reference transmission line modulator equivalent circuit:

- the input and output optical ports are swapped with respect to the co-propagating case;
- the optical wave has an unchanged propagation direction while the microwave signal is generated at the load terminal and collected at the source one.

The analysis performed is similar to the one discussed in the co-propagating case.

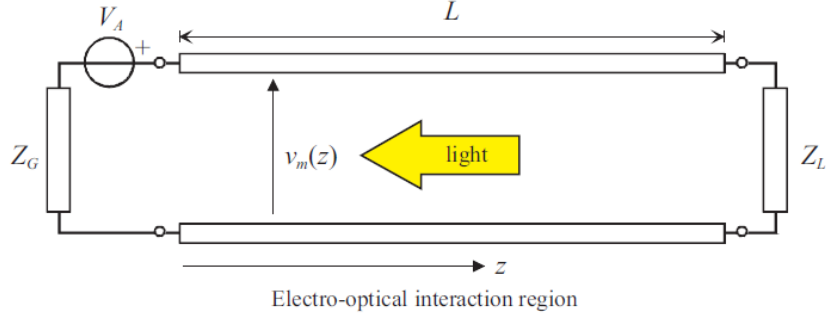


Figure 1.3. Counter-propagating Circuit Schematic.

Referring to the first equivalent circuit Fig.1.3, the RF voltage seen at the generic position z has to be reformulated since the phase modulated optical signal propagates in an opposite direction with respect to the previous case. It is applied at the end of the active region in position $z = L$ and propagates towards $z = 0$). $v_m(z, t(z))$ becomes:

$$v_m(z, t(z)) = v_m(z, t_0 + \frac{L-z}{v_o}) = V(z)e^{j\omega t_0}e^{j\beta_o(L-z)}$$

where the line voltage $V(z)$ does not change. Following the same steps, it is possible to find the total phase shift $\Delta\Phi_{ct}$ integrating the induced $\Delta\beta$ over the interval $[0, L]$

$$\Delta\Phi_{ct}(f, t_0) = \int_0^L \Delta\beta dz = \frac{\pi}{\lambda_0} \frac{n^3 r \Gamma}{G} E_G \frac{Z_{in}}{Z_i n + Z_G} \cdot \int_0^L \frac{(Z_L + Z_0)e^{\gamma_m(L-z)} + (Z_L - Z_0)e^{-\gamma_m(L-z)}}{(Z_L + Z_0)e^{\gamma_m L} + (Z_L - Z_0)e^{-\gamma_m L}} e^{j\omega t_0} e^{j\beta_o(L-z)} dz.$$

Defining

$$F(u_{\pm}) = \frac{1 - u_{\pm}}{u_{\pm}}$$

where

$$u_{\pm} = (\pm\gamma_m - j\beta_o)L = j(\pm\beta_m - \beta_o)L \pm \alpha_m L = \pm\alpha_m L + j\frac{\omega}{c_0}(\pm n_m - n_o)L.$$

The total phase shift becomes:

$$\Delta\Phi_{co}(f, t_0) = \frac{\pi}{\lambda_0} \frac{n^3 r \Gamma L}{G} E_G \frac{Z_{in}}{Z_i n + Z_G} \cdot \frac{(Z_L + Z_0)F(u_+)e^{j\gamma_m L} + (Z_L - Z_0)F(u_-)e^{-j\gamma_m L}}{(Z_L + Z_0)e^{u_+} + (Z_L - Z_0)e^{u_-}} e^{j\omega t_0}. \quad (1.15)$$

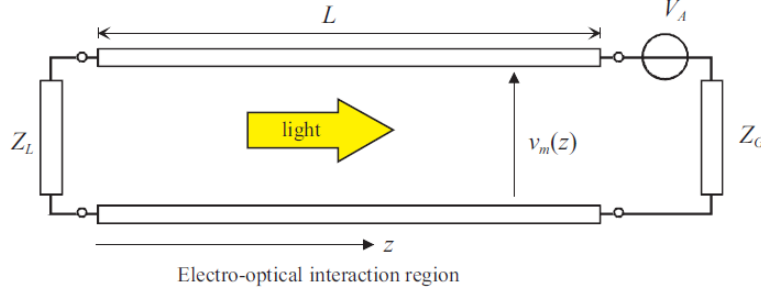


Figure 1.4. Counter-propagating Circuit Schematic.

Instead, using as reference the second equivalent circuit Fig. 1.4, the line voltage has to be reformulated as follows:

$$V(z, t) = E_G \frac{Z_{in}}{Z_g + Z_{in}} \frac{(Z_L + Z_0)e^{\gamma_m z} + (Z_L - Z_0)e^{-\gamma_m z}}{(Z_L + Z_0)e^{\gamma_m L} + (Z_L - Z_0)e^{-\gamma_m L}} e^{j\omega t}$$

and so $v_m(z, t(z))$ becomes:

$$v_m(z, t(z)) = E_G \frac{Z_{in}}{Z_g + Z_{in}} \frac{(Z_L + Z_0)e^{\gamma_m z} + (Z_L - Z_0)e^{-\gamma_m z}}{(Z_L + Z_0)e^{\gamma_m L} + (Z_L - Z_0)e^{-\gamma_m L}} e^{j\omega t} e^{j\beta_0 z}.$$

Taking into account the previous expression, it is possible to evaluate the total phase shift integrating the resulting $\Delta\beta$ over the total length of the phase modulating arm. The resulting $\Delta\Phi_{ct}$ is

$$\Delta\Phi_{ct}(f, t_0) = \int_0^L \Delta\beta dz = \frac{\pi}{\lambda_0} \frac{n^3 r \Gamma}{G} E_G \frac{Z_{in}}{Z_i n + Z_G} \cdot \int_0^L \frac{(Z_L + Z_0)e^{\gamma_m z} + (Z_L - Z_0)e^{-\gamma_m z}}{(Z_L + Z_0)e^{\gamma_m L} + (Z_L - Z_0)e^{-\gamma_m L}} e^{j\omega t_0} e^{j\beta_0 z} dz.$$

$$\Delta\Phi_{co}(f, t_0) = \frac{\pi n^3 r \Gamma L}{\lambda_0 G} E_G \frac{Z_{in}}{Z_i n + Z_G} \cdot \frac{(Z_L + Z_0)F(u_+)e^{j\gamma_m L} + (Z_L - Z_0)F(u_-)e^{-j\gamma_m L}}{(Z_L + Z_0)e^{u_+} + (Z_L - Z_0)e^{u_-}} e^{j\omega t_0}.$$

which coincides with the one evaluated in (1.15).

1.3.3 Frequency Response

[2][3] As already discussed in the lumped case, the frequency response can be analysed studying the behaviour of the modulator index $m(\omega)$ where

$$m(\omega) = \left| \frac{\Delta\Phi(\omega)}{\Delta\Phi(0)} \right|.$$

It can be mainly limited by three factors:

- the velocity mismatch between the optical and the RF signals ($\Delta n = n_m - n_o \neq 0$);
- the RF losses of the modulator line;
- the impedance mismatch of the transmission line with respect to the generator and the load.

Considering the co-propagating case, the expression of the the the total induced phase shift with respect to a reference time t , in absence of losses ($\alpha_m = 0$) and impedance mismatch ($Z_L = Z_G = Z_0$) becomes:

$$\Delta\Phi_{co}(\omega) = -\frac{\pi n^3 r \Gamma L}{\lambda_0 G} E_G \frac{Z_0}{Z_0 + Z_G} \text{sinc} \left[\frac{j\omega}{2c_0} (n_m - n_o) L \right] e^{\frac{j\omega}{2c_0} (n_m - n_o) L} e^{j\omega t_0}.$$

and so

$$m(\omega) = |F(u_+)| = \left| \frac{\sin(U)}{U} \right|$$

where

$$U = \frac{j\omega}{2c_0} (n_m - n_o) L. \quad (1.16)$$

Imposing the following conditions

$$m_{op}(f_{3dB,op})|_{dB} = 10 \log_{10}[m(f_{3dB,op})] = -3dB \quad (1.17)$$

$$m_{el}(f_{3dB,el})|_{dB} = 20 \log_{10}[m(f_{3dB,el})] - 3dB \quad (1.18)$$

it is possible to obtain $U_{3dB,op} = 1.89$ and $U_{3dB,el} = 1.39$ and so, from (1.16), $f_{3dB,el}$ and $f_{3dB,op}$ which are respectively the electrical and optical 3dB Bandwidth

$$f_{3dB,op}L = \frac{1.89c_0}{\pi(n_m - n_o)} \text{GHz} \cdot \text{m} \quad (1.19)$$

$$f_{3dB,el}L = \frac{1.39c_0}{\pi(n_m - n_o)} \text{GHz} \cdot \text{m} \quad (1.20)$$

It can be noticed from (1.19) and (1.20) that the velocity mismatch causes a reduction of the bandwidth.

In the case of nearly velocity matching (5% of velocity mismatch) and perfect impedance matching ($Z_L = Z_G = Z_0$), $\Delta\Phi_{co}(\omega)$ becomes

$$\Delta\Phi_{co}(\omega) = -\frac{\pi}{\lambda_0} \frac{n^3 r \Gamma L}{G} E_G \frac{Z_0}{Z_0 + Z_G} \frac{1 - e^{-\alpha_m L}}{\alpha_m L} e^{j\omega t_0}$$

and so

$$m(\omega) = e^{-W} \left| \frac{\sinh(W)}{W} \right|$$

where

$$W = \frac{\alpha_m(f)L}{2} = \frac{\alpha_m(f_0)L}{2} \sqrt{\frac{f}{f_0}} \quad (1.21)$$

Imposing (1.17) and (1.18), it is possible to fine the electrical and optical 3dB Bandwidth in the presence of RF losses ($W_{3dB,el} = 0.368$ and $W_{3dB,op} = 0.794$). Substituting these two value in equation (1.21), it is possible to find the total line attenuation corresponding to the optical and electrical bandwidth ($\alpha_m(f_{3dB,op})$ and $\alpha_m(f_{3dB,el})$)

$$\frac{\alpha_m(f_{3dB,op})L}{2} = 0.794$$

$$\alpha_m(f_{3dB,op})L = 1.588$$

$$\alpha_m(f_{3dB,op})L|_{dB} = 13.79\text{dB}$$

$$\frac{\alpha_m(f_{3dB,el})L}{2} = 0.368$$

$$\alpha_m(f_{3\text{dB},el})L = 0.736$$

$$\alpha_m(f_{3\text{dB},el})L|_{\text{dB}} = 6.393\text{dB}$$

The effect of losses are a reduction of the electrical and optical 3dB Bandwidth and the filling of response zeros, they can be the main cause of a bandwidth reduction in high speed modulators which turns into a reduction of the electro-optic interaction.

In presence of impedance mismatch but no losses or velocity mismatch

$$\Delta\Phi_{co}(\omega) = -\frac{\pi}{\lambda_0} \frac{n^3 r \Gamma L}{G} E_G \frac{Z_{in}}{Z_{in} + Z_G} \frac{F(u_-)}{e^{-2j\beta_m L}}$$

and so

$$m(\omega) = \frac{R_L + R_G}{R_L} \left| \frac{Z_{in}}{Z_{in} + Z_G} \frac{F(u_-)}{e^{-2j\beta_m L}} \right|$$

where

$$u_- = -2j\beta_m L.$$

Impedance mismatch causes multiple reflections of the microwave signal and so the effective voltage on the electrodes changes as a function of frequency, which results in ripple in the optical response.

Counter propagating frequency response

To understand the counter-propagating frequency response a comparison with the results obtained in the co-propagating case is performed.

The total induced phase shift for co-propagating signals with respect to a fixed time t_0 in the case of perfectly matched load and transmission line is expressed as follows:

$$\begin{aligned} \Delta\Phi_{co}(f) &= -\frac{\pi}{\lambda_0} \frac{n^3 r \Gamma L}{G} E_G \frac{Z_0}{Z_0 + Z_G} \frac{F(u_+)}{e^{u_+}} = \\ &= \Delta\Phi(0) e^{\frac{u_+}{2}} \frac{\sin \left[-j \frac{\alpha_m L}{2} + \frac{\pi f}{c_0} (n_m - n_o) L \right]}{-j \frac{\alpha_m L}{2} + \frac{\pi f}{c_0} (n_m - n_o) L} \end{aligned} \quad (1.22)$$

where

$$\Delta\Phi(0) = -\frac{\pi}{\lambda_0} \frac{n^3 r \Gamma L}{G} E_G \frac{Z_0}{Z_0 + Z_G}.$$

In the counter propagating case instead

$$\begin{aligned}
 \Delta\Phi_{ct}(f) &= -\frac{\pi}{\lambda_0} \frac{n^3 r \Gamma L}{G} E_G \frac{Z_0}{Z_0 + Z_G} \frac{F(u_+)}{e^{u_+}} e^{\gamma_m L} = \\
 &= \Delta\Phi(0) e^{\frac{u_+}{2}} \frac{\sin \left[-j \frac{\alpha_m L}{2} + \frac{\pi f}{c_0} (n_m + n_o) L \right]}{-j \frac{\alpha_m L}{2} + \frac{\pi f}{c_0} (n_m + n_o) L} e^{\frac{\gamma_m + j 3 \beta_o}{2} L}. \quad (1.23)
 \end{aligned}$$

If the losses are negligible, (1.22) and (1.23) become:

$$\begin{aligned}
 \Delta\Phi_{co}(f) &= \Delta\Phi(0) e^{-j \frac{\pi f}{c_0} (n_m - n_o) L} \operatorname{sinc} \left[\frac{\pi f}{c_0} (n_m - n_o) L \right] \\
 \Delta\Phi_{ct}(f) &= \Delta\Phi(0) e^{-j \frac{\pi f}{c_0} (n_m + 3n_o) L} \operatorname{sinc} \left[\frac{\pi f}{c_0} (n_m + n_o) L \right].
 \end{aligned}$$

Looking at the sinc argument in the two cases, it can be noticed that for co-propagating waves a velocity matching and so a synchronization of the RF and optical signals can be achieved since the argument is proportional to a difference of refractive indexes, while in the counter-propagating case a synchronization of the two signals is impossible due to the presence of a sum of the two real and positive values n_m and n_o .

A further confirmation comes looking at the expression of the optical response 3dB Bandwidth

$$\begin{aligned}
 f_{3dB,co} &= \frac{1.39c_0}{\pi(n_m - n_o)L} \\
 f_{3dB,ct} &= \frac{1.39c_0}{\pi(n_m + n_o)L}
 \end{aligned}$$

in the case of counter-propagating waves the bandwidth is furtherly reduced with respect to the one obtained for co-propagating signals and so the performances are even worse.

1.4 Chirp Model

[2] Referring to the lumped case, in addition to the amplitude modulation performed by output optical combiner, a spurious phase modulation is present at the output of the EO Mach Zehnder Modulator due to geometrical factor rather than physical parameters.

To evaluate the instantaneous frequency deviation a time dependence is introduced in (1.4)

$$\begin{aligned} b'_1 &= e^{2j\phi_{sp}} e^{-jk_0L} \left[\alpha e^{-j\Delta\Phi_U(t)} + (1-\alpha) e^{-j\Delta\Phi_L(t)} a_1 \right] = \\ &= K \left[\alpha e^{-j\Delta\Phi_U(t)} + (1-\alpha) e^{-j\Delta\Phi_L(t)} a_1 \right] \end{aligned}$$

where $K = a_1 e^{2j\phi_{sp}} e^{-jk_0L}$ is a time independent constant. The phase of the output signal is obtained as

$$\begin{aligned} \phi(t) &= -\tan^{-1} \left[\frac{\text{Im}(b'_1/K)}{\text{Re}(b'_1/K)} \right] \\ \phi(t) &= \tan^{-1} \left[\frac{\alpha \sin(\Delta\Phi_U(t)) + (1-\alpha) \sin(\Delta\Phi_L(t))}{\alpha \cos(\Delta\Phi_U(t)) + (1-\alpha) \cos(\Delta\Phi_L(t))} \right] \end{aligned} \quad (1.24)$$

$\Delta f(t)$ is obtained deriving (1.24) with respect to the time

$$\Delta f(t) = \frac{1}{2\pi} \frac{d\phi(t)}{dt} = \frac{1}{2\pi} \frac{d}{dt} \tan^{-1} \left[\frac{\alpha \sin(\Delta\Phi_U(t)) + (1-\alpha) \sin(\Delta\Phi_L(t))}{\alpha \cos(\Delta\Phi_U(t)) + (1-\alpha) \cos(\Delta\Phi_L(t))} \right].$$

In the case of symmetrical splitter and combiner (i.e. $\alpha = 1/2$) $\Delta f(t)$ becomes

$$\begin{aligned} \Delta f(t) &= \frac{1}{2\pi} \frac{d}{dt} \tan^{-1} \left[\frac{\sin(\Delta\Phi_U(t)) + \sin(\Delta\Phi_L(t))}{\cos(\Delta\Phi_U(t)) + \cos(\Delta\Phi_L(t))} \right] = \\ &= \frac{1}{2\pi} \frac{d}{dt} \tan^{-1} \left[\frac{2 \sin\left(\frac{\Delta\Phi_U + \Delta\Phi_L}{2}\right) \cos\left(\frac{\Delta\Phi_U - \Delta\Phi_L}{2}\right)}{2 \cos\left(\frac{\Delta\Phi_U + \Delta\Phi_L}{2}\right) \cos\left(\frac{\Delta\Phi_U - \Delta\Phi_L}{2}\right)} \right] = \\ &= \frac{1}{2\pi} \frac{d}{dt} \tan^{-1} \left[\tan \frac{\Delta\Phi_U + \Delta\Phi_L}{2} \right] = \frac{1}{4\pi} \frac{d(\Delta\Phi_U + \Delta\Phi_L)}{dt} \end{aligned}$$

Substituting the expressions of $\Delta\Phi_U$ and $\Delta\Phi_L$ (1.6)

$$\Delta f(t) = \frac{1}{4} \left[\frac{1}{V_{\pi U}} \frac{dv_{inU}}{dt} - \frac{1}{V_{\pi L}} \frac{dv_{inL}}{dt} \right]. \quad (1.25)$$

While the result of the amplitude modulation is

$$P_{out} = \frac{1}{2} \eta [1 + \cos(\Delta\Phi_U(t) - \Delta\Phi_L(t))]$$

deriving with respect to time

$$\begin{aligned} \frac{1}{P_{out}} \frac{dP_{out}}{dt} &= \pi \frac{\frac{1}{2} \eta \sin(\Delta\Phi_U - \Delta\Phi_L)}{\frac{1}{2} \eta [1 + \cos(\Delta\Phi_U - \Delta\Phi_L)]} \left[\frac{1}{V_{\pi U}} \frac{dv_{inU}}{dt} + \frac{1}{V_{\pi L}} \frac{dv_{inL}}{dt} \right] \\ &= \tan \left(\frac{\Delta\Phi_U(t) - \Delta\Phi_L(t)}{2} \right) \left[\frac{1}{V_{\pi U}} \frac{dv_{inU}}{dt} + \frac{1}{V_{\pi L}} \frac{dv_{inL}}{dt} \right]. \end{aligned} \quad (1.26)$$

The instantaneous frequency deviation is described by the Henry chirp parameter α_H

$$\alpha_H = \frac{4\pi\Delta f}{\frac{1}{P_{out}} \frac{dP_{out}}{dt}} \quad (1.27)$$

substituting (1.25) and (1.26) in (1.27)

$$\alpha_H = \frac{\frac{1}{V_{\pi U}} \frac{dv_{inU}}{dt} - \frac{1}{V_{\pi L}} \frac{dv_{inL}}{dt}}{\frac{1}{V_{\pi U}} \frac{dv_{inU}}{dt} + \frac{1}{V_{\pi L}} \frac{dv_{inL}}{dt}} \cot \left(\frac{\Delta\Phi_U(t) - \Delta\Phi_L(t)}{2} \right).$$

It is a function of time which values might be positive or negative according to the modulator parameters and the driving voltages. If $v_{inU} = v_{inL} = v_{in}$, α_H becomes:

$$\alpha_H = \frac{V_{\pi U} - V_{\pi L}}{V_{\pi U} + V_{\pi L}} \cot \left(\frac{\Delta\Phi_U(t) - \Delta\Phi_L(t)}{2} \right) = \frac{V_{\pi U} - V_{\pi L}}{V_{\pi U} + V_{\pi L}} \cot \left(\frac{\pi}{2} \frac{v_{in}(t)}{V_{\pi}} \right)$$

where V_{π} has been defined as

$$V_{\pi} = \frac{V_{\pi U} V_{\pi L}}{V_{\pi U} + V_{\pi L}}.$$

In small signal conditions

$$\alpha_H = \frac{V_{\pi U} - V_{\pi L}}{V_{\pi U} + V_{\pi L}} \cot \left(\frac{\pi}{2} \frac{V_{in}(t)}{V_{\pi}} \right) \quad (1.28)$$

where

$$v_{in}(t) = V_{in} + \hat{v}_{in}(t) \approx V_{in}.$$

It can be noticed from (1.28) that α_H is a constant in small signal condition and its value can be tuned by the value of $\cot((\pi/2)(V_{in}(t)/V_{\pi}))$. Biasing the device at the optimum point for linearity (i.e. $V_{in} = V_{\pi}/2$), $\cot((\pi/2)(V_{in}(t)/V_{\pi}))$ is equal to 1 and the chirp just depends on the unbalance between the modulator upper and lower arms, while if the modulator is completely symmetrical $V_{\pi U} = V_{\pi L}$ and the chirp is null at any applied bias point.

Chapter 2

EO Mach-Zehnder modulator: Multi-Sectional Model

2.1 Introduction

In the previous chapter, basic theoretical knowledge on a Mach Zehnder modulator was proposed, the device was analysed when it is considered lumped or travelling wave, presenting some parameters that are fundamental for the description of its behaviour. The aim of this chapter is to propose a model that is realizable within the framework of a microwave CAD suite allowing for the optimization of the geometrical parameters, time-domain analysis, small-signal and large signal analysis. In order to guarantee the compatibility of the device with the CAD requirements some solutions are adopted, the overall design is divided in blokes and the optical signals are represented as pseudo-electrical signals. Finally few implementation details regarding the block models and their realizations are presented.

2.2 Modelling

[2][3][5] In the previous chapter the Mach-Zehnder amplitude modulator has been presented as a structure made of three sections:

- an Y-junction beam splitter;
- an Y-junction beam combiner;
- a region made of two arms providing a phase shift between the splitted signals if required.

The phase delay in the inbetween region is given by the interaction between the optical signal travelling in the two arms of the modulator and a microwave signal guided by an RF transmission line. Its magnitude depends mainly on three factors: the line length, the mismatch between the optical and the RF signal velocities and the microwave electric field. In the development of this kind of devices in an RF CAD environment some issues have to be considered. First of all, the overall structure is dispersive and non-linear, it cannot be directly handled by a RF circuit or system simulators which supports only linear and dispersive or memoryless and non-linear devices. In order to overcome this problem, the modulator has been divided in two blocks:

- the Phase-Modulator Block (PM block) representing the phase shifting arms;
- the Interference Block (AM block) representing the Y-combiner.

Another concern is to find a way to describe optical signals in a microwave CAD environment since optical components does not exist in this kind of tool. The adopted solution associates electrical variables (ports) to optical signals. For instance, in the frequency domain, the optical signal power and slowly varying phase are expressed as RF currents having the same frequency as the input RF signal.

Finally, the electro-optical phase shift has to be described no more in term of generator and load impedances but as a function of the voltage at the input and output sections of the interaction region. This requirement comes from the need to have a model compatible with a circuit simulator based, for example, on nodal analysis.

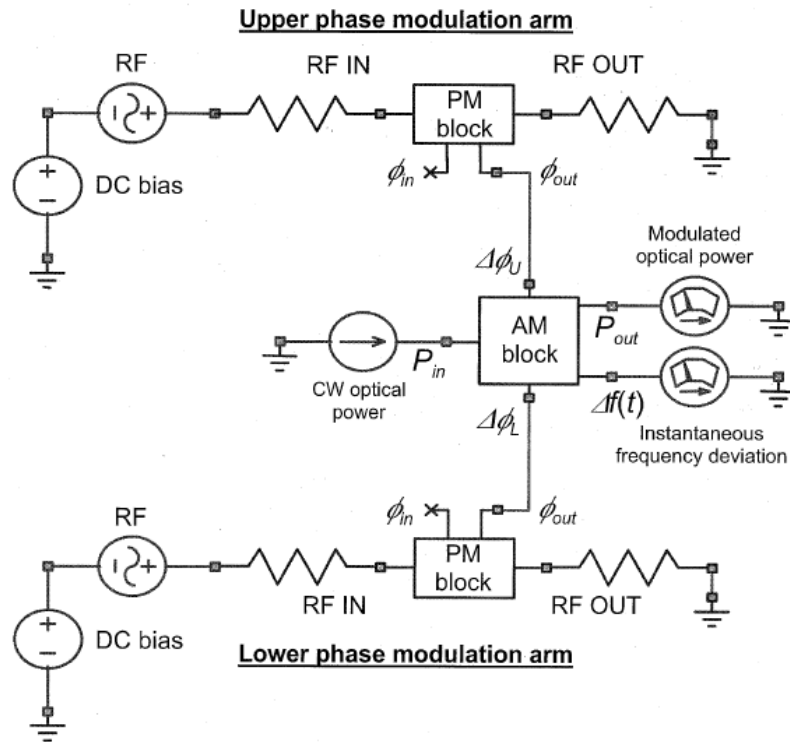


Figure 2.1. [5] Schematic of a Mach-Zehnder Amplitude Modulator.

2.3 Phase-Modulation Block

[2][3][5] The PM block is a four port block model with two electrical ports and two optical ones. The driving measures are the electrical voltages applied at the RF ports while an input phase delay (Φ_{in}) coming from other circuit elements and the total phase modulation (Φ_{out}) are the optical measures expressed as currents (respectively I_{in} and I_{out}).

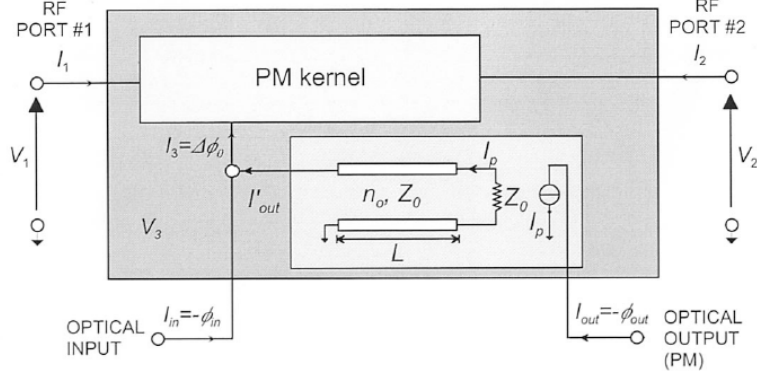


Figure 2.2. [3]Phase-Modulation Block.

The quantity to measure is the electro-optical phase shift $\Delta\Phi_{out}$ expressed as a function of the voltage at the input section of the interaction region between the optical and the RF signals ($V_1 = V(z_1)$ where $z_1 = 0$) and the voltage at the output one ($V_2 = V(z_2)$ where $z_2 = L$).

2.3.1 Mathematical Formulation

[3] The first step to begin the development of the corresponding CAD model is the study of a more general mathematical reformulation of the previously used formalism. The model implemented has to be *stand alone* i.e. independent from any assumption on external conditions imposed by the circuit network connected to it.

As already seen, the interaction region between the optical and microwave signal can be modelled simply as a transmission line of length L and it is analysed in term of active device electrode voltage distribution but, due to the previous statement, the co-propagating and counter-propagating operating conditions are unified and do not require a separate discussion any more.

Starting from the expression of the voltage at a generic section z of a homogeneous transmission line,

$$V(z) = V_1^+ e^{-\gamma_m z} + V_1^- e^{\gamma_m z} \quad (2.1)$$

where V_1^+ and V_1^- , respectively, the progressive and regressive voltage measured at $z = 0$, it is possible to find the input and output voltages

$$\begin{cases} V_1 = V_1^+ + V_1^- \\ V_2 = V_1^+ \exp(-\gamma_m L) + V_1^- \exp(\gamma_m L) \end{cases}$$

where L is the line length.

To obtain the line voltage $V(z)$ as a function of V_1 and V_2 this system has to be inverted so that it is possible to find V_1^+ and V_1^- , the solution in matrix form is:

$$\begin{bmatrix} V_1^+ \\ V_1^- \end{bmatrix} = \frac{1}{\exp(\gamma_m L) - \exp(-\gamma_m L)} \begin{bmatrix} \exp(\gamma_m L) & -1 \\ \exp(-\gamma_m L) & 1 \end{bmatrix} \begin{bmatrix} V_1 \\ V_2 \end{bmatrix}$$

and then considering also the effect of the propagation in time domain

$$V(z, t) = V(z)e^{j\omega t} = \frac{(V_1 e^{\gamma_m L} - V_2)e^{-\gamma_m z} + (V_2 - V_1 e^{-\gamma_m L})e^{\gamma_m z}}{e^{\gamma_m L} - e^{-\gamma_m L}} e^{j\omega t}.$$

From this is possible to measure the line voltage seen by the optical field at section z at t (reference time). This voltage is:

$$V_\mu(z, t(z)) = V\left(z, t_0 + \frac{z}{v_o}\right) = V(z)e^{j\omega\left(t_0 - \frac{z}{v_o}\right)} = V(z)e^{j\omega t} e^{j\beta_0 z} \quad (2.2)$$

where $t_0 = 0$ is the reference time and $v_o = n_0/c$ (c is the speed of light and n_0 the optical refractive index).

Substituting the voltage in (2.2) in (1.1), the electro-optic induced change in the refractive index is obtained as follows:

$$\Delta n = -\frac{1}{2} \frac{n^3 r \Gamma}{G} V(z) e^{j\omega t} e^{j\beta_0 z}. \quad (2.3)$$

Following the same procedure done in Ch.1, the global induced phase shift is obtained integrating the variation of the refractive index along the active region as

$$\Delta\Phi(f, t_0) = \frac{2\pi}{\lambda_0} \int_0^L \Delta n(z) dz$$

Substituting (2.3) and (2.1) the result is

$$\begin{aligned} \Delta\Phi(f, t_0) &= -\frac{\pi}{\lambda_0} \frac{n^3 r \Gamma}{G} e^{j\omega t_0} \int_0^L V(z) e^{j\beta_0 z} dz = \\ &= -\frac{\pi}{\lambda_0} \frac{n^3 r \Gamma}{G} e^{j\omega t_0} \int_0^L (V_1^+ e^{-\gamma_m z + j\beta_0 z} + V_1^- e^{\gamma_m z + j\beta_0 z}) dz \end{aligned}$$

Finally, defining

$$\nu_\pm = (\pm\gamma_m + j\beta_0)L$$

and

$$\Psi(\nu_\pm) = \frac{1}{L} \int_0^L e^{\nu_\pm \frac{z}{L}} dz = \frac{1}{\nu_\pm} (1 - e^{\nu_\pm}).$$

the phase shift in term of progressive and regressive wave is obtained as:

$$\Delta\Phi(f, t_0) = -\frac{\pi}{\lambda_0} \frac{n^3 r \Gamma L}{G} e^{j\omega t_0} (V_1^+ \Psi(\nu_-) + V_1^- \Psi(\nu_+)).$$

In order to find the phase shift as a function of the line input and output voltages an additional step is required. Considering the functions

$$\begin{cases} \zeta_1(f) = \frac{\Psi(\nu_-)e^{\gamma_m L} - \Psi(\nu_+)e^{-\gamma_m L}}{e^{\gamma_m L} - e^{-\gamma_m L}} \\ \zeta_2(f) = \frac{-\Psi(\nu_-) + \Psi(\nu_+)}{e^{\gamma_m L} - e^{-\gamma_m L}} \end{cases}$$

which are a linear combination of the Ψ function, $\Delta\Phi(f, t_0)$ becomes:

$$\Delta\Phi(f, t_0) = -\frac{\pi}{\lambda_0} \frac{n^3 r \Gamma L}{G} e^{j\omega t_0} (V_1 \zeta_1(f) + V_2 \zeta_2(f)).$$

DC finite resistance

Even though the transmission line model used to describe the behaviour of the metal electrodes supposes that their conductivity is infinite (i.e. they can be seen as short circuits), the active region is characterized by a small parasitic resistance which may influence the value of $V_{\pi, DC}$ (i.e. the optimum bias point for linearity when a small signal analysis is performed). Generally this resistance can be neglected if an accurate analysis is not required but in low power structures, in order to reduce the *ON – OFF* voltage, the active region length L is increased and it turns in an increase of the active region resistance due to its linear dependence on the length. The result is that the parasitic resistance R_{DC} cannot be neglected anymore.

The strategy adopted to implement the presence of R_{DC} and its influence on the overall performance is simply to replace the transmission line with its series resistor at DC which does not require to modify the transmission line model developed so far or the introduction of an *ad hoc* frequency-independent attenuation constant. The value of R_{DC} is obtained as

$$R_{DC} = R \cdot L$$

where R is the resistance per unit of length. In order to formulate the optical response in a way consistent with the formalism developed so far, the voltage distribution along the resistor has to be evaluated. Considering an ohmic conductor of length L

$$V(z) = V_1 - \frac{V_1 - V_2}{L} z \quad (2.4)$$

where $z \in [0, L]$, V_1 and V_2 are the resistor port voltages such that

$$V_1 - V_2 = R_{DC}I.$$

I as the current flowing in the resistor.

It is possible to evaluate the induced phase shift at DC substituting (2.4) in the expression of $\Delta\Phi(0, t_0)$

$$\begin{aligned} \Delta\Phi(0, t_0) &= \lim_{f \rightarrow 0} -\frac{\pi}{\lambda_0} \frac{n^3 r \Gamma}{G} e^{j\omega t_0} \int_0^L V(z) e^{j\beta_0 z} dz = \\ &= -\frac{\pi}{\lambda_0} \frac{n^3 r \Gamma}{G} \int_0^L \left(V_1 - \frac{V_1 - V_2}{L} z \right) dz = \\ \Delta\Phi(0, t_0) &= -\frac{\pi}{\lambda_0} \frac{n^3 r \Gamma}{2G} (V_1 - V_2)L. \end{aligned} \quad (2.5)$$

Equation (2.5) becomes equal to the induced phase shift of a lumped ideal modulator (1.2) when $R_{DC} \approx 0$ (i.e. $V_1 = V_2 = V$)

$$\Delta\Phi(0, t_0) = -\frac{\pi}{\lambda_0} \frac{n^3 r \Gamma}{G} LV$$

2.3.2 Modelling

[2][3][5] Starting from the model just explained, the PM block has been developed in the CAD environment It is in turn divided in two sub-component:

- a modulating core which provides the undelayed (i.e. referring to the input of the interaction section) electro-optical phase modulation (PM Kernel);
- an optical delay line which adjust the optical phase shift according to the multisectional requirement of the device.

Phase Modulating Kernel

The PM Modulating Kernel is a linear three-port device characterized by two electrical input and one optical output. At the optical port (port 3) is present the undelayed optical phase shift ($\Delta\Phi_0$) as a function of the RF signal (i.e. the voltages at port 1 V_1 and 2 V_2). The whole admittance matrix in the frequency domain is:

$$\begin{bmatrix} I_1 \\ I_2 \\ I_3 \end{bmatrix} = \begin{bmatrix} Y_{11} & Y_{12} & 0 \\ Y_{21} & Y_{22} & 0 \\ \zeta_1 & \zeta_2 & 0 \end{bmatrix} \begin{bmatrix} V_1 \\ V_2 \\ V_3 \end{bmatrix}$$

where

$$Y_{RF} = \begin{bmatrix} Y_{11} & Y_{12} \\ Y_{21} & Y_{22} \end{bmatrix}$$

is the admittance matrix of the transmission line section and

$$Y_{\Delta\Phi} = [\zeta_1 \zeta_2]$$

is the sub-matrix related to the optical phase shift. It can be noticed the presence of the zero column in the admittance matrix \mathbf{Y} represents the impossibility of the voltage at port 3 (the optical one) to influence the electrical circuit part. Since the interaction region is modelled as a lossy transmission line, the RF admittance matrix can be evaluated as:

$$Y_{RF} = Y_0(I - S) \cdot (I + S)^{-1}$$

where Y_0 is the characteristic admittance and

$$S = \begin{bmatrix} 0 & e^{-\gamma_m L} \\ e^{\gamma_m L} & 0 \end{bmatrix}$$

and so

$$Y_{RF} = \frac{Y_0}{1 - e^{-2\gamma_m L}} \begin{bmatrix} 1 + e^{-2\gamma_m L} & -2e^{-2\gamma_m L} \\ -2e^{-2\gamma_m L} & 1 + e^{-2\gamma_m L} \end{bmatrix} \quad (2.6)$$

valid for $f \neq 0$. When the frequency is zero, Y_{RF} is equal to

$$Y_{RF} = \begin{bmatrix} \frac{1}{R_{DC}} & -\frac{1}{R_{DC}} \\ -\frac{1}{R_{DC}} & \frac{1}{R_{DC}} \end{bmatrix}$$

$Y_{\Delta\Phi}$ instead represents an ideal linear controlled current generator (*VCCS*) where $Y_{33} = 0$ has been imposed. It generates the current I_3 which is the electrical variable corresponding to the undelayed phase shift. Starting from:

$$I_3 = [\zeta_1 \zeta_2] \begin{bmatrix} V_1 \\ V_2 \end{bmatrix}$$

where

$$\begin{cases} \zeta_1(f) = \frac{\Psi(\nu_-)e^{\gamma_m L} - \Psi(\nu_+)e^{-\gamma_m L}}{e^{\gamma_m L} - e^{-\gamma_m L}} \\ \zeta_2(f) = \frac{-\Psi(\nu_-) + \Psi(\nu_+)}{e^{\gamma_m L} - e^{-\gamma_m L}} \end{cases}$$

$$\Psi(\nu_{\pm}) = \frac{1}{\nu_{\pm}}(1 - e^{\nu_{\pm}}),$$

$$\nu_{\pm} = (\pm\gamma_m + j\beta_0)L$$

neglecting the dependence at the reference time t_0 , the phase shift is obtained as:

$$I_3 = \Delta\Phi_0(f, t_0) = -\frac{\pi}{\lambda_0} \frac{n^3 r \Gamma L}{G} (V_1 \zeta_1(f) + V_2 \zeta_2(f))$$

Substituting the value of the *ON – OFF* voltage V_{π} , the final result is:

$$Y_{\Delta\phi_0} = \frac{\pi}{V_{\pi}} [\zeta_1 \zeta_2]$$

.

Optical Phase line

It is a two-port device modelled as an ideal lossless transmission line terminated on matched loads to avoid back reflection, an output controlled current source guarantees complete decoupling from subsequent stages and makes the line unidirectional. Since the phase signal is not a real phase signal but a current, this device can be connected to those elements that are contained in other modulation blocks like ideal current generators, current meters or other optical lines.

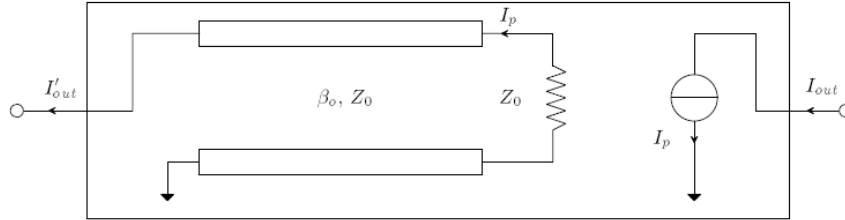


Figure 2.3. [3]Optical Phase Line.

The physical phenomenon modelled is the delay of the induced phase shift due to the finite velocity of the optical beam. The input and output phase modulation are related as follow

$$\Phi_{out} = (\Phi_{in} + \Delta\Phi_0)e^{-j\omega\frac{n_o}{c}L} = \Phi_{in}e^{-j\omega\frac{n_o}{c}L} + \Delta\Phi$$

The corresponding electrical formulation is

$$I_{out} = I'_{out}e^{-j\beta_0L} = (-I_{in} + I_3)e^{-j\beta_0L}$$

where $\beta_0 = \omega\frac{n_o}{c}$.

2.4 AM Block

[2][3][5] The interference block is a five port device that models the behaviour of an output optical combiner.

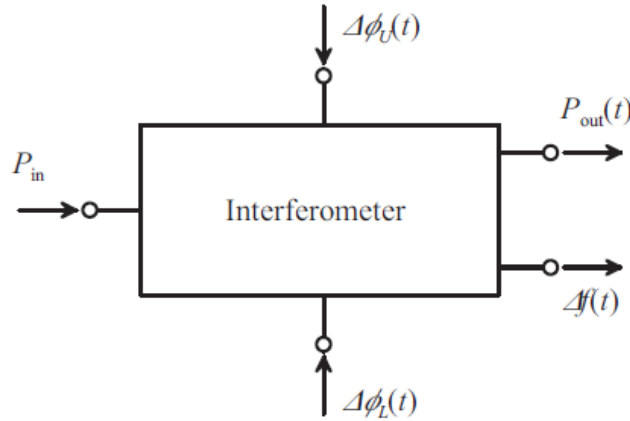


Figure 2.4. [3]Interferometer.

There are three input ports and two output ones where two of the optical inputs are $\Delta\Phi_U$ and $\Delta\Phi_L$, respectively the total phase shift coming from the lower and upper Mach-Zehnder modulator arm and are represented as currents, the remaining optical input represents the input optical power P_{in} as a current. The two optical outputs represent the output optical power resulting from the amplitude modulation i.e. interference of the the signals coming from the two arms and the instantaneous frequency deviation (chirp) $\Delta f(t)$, they are as well described as currents.

The aim of this section is to provide a mathematical formulation of the output optical power intensity and the instantaneous frequency chirping as a function of the splitting ratios of the Y-junctions and of the interferometer arms asymmetry.

The amplitude of the output optical field a_{out} is defined as follows:

$$a_{out} = \frac{a_{in}\sqrt{\eta}}{\sqrt{2}}[\sqrt{\alpha}e^{j\Delta\Phi_U} + \sqrt{1-\alpha}e^{j\Delta\Phi_L}] \quad (2.7)$$

where $\eta = P_{in}/P_{out}$ is the overall power efficiency in absence of modulation and $\alpha = P_U/P_T$ is the asymmetry factor equal to the power flowing in the upper (P_U) arm and the transmitted power ($P_T = \eta P_{in}$), these two parameters make possible to take into account the splitting ratio effect.

It is possible to find the normalized output power from (2.7) as:

$$\begin{aligned} P &= \left\| \frac{a_{out}}{a_{in}} \right\|^2 = \frac{\eta}{2} [\sqrt{\alpha}e^{j\Delta\Phi_U} + \sqrt{1-\alpha}e^{j\Delta\Phi_L}] [\sqrt{\alpha}e^{-j\Delta\Phi_U} + \sqrt{1-\alpha}e^{-j\Delta\Phi_L}] \\ &= \frac{\eta}{2} + 2\eta\sqrt{\alpha - \alpha^2} \frac{e^{j(\Delta\Phi_U - \Delta\Phi_L)}}{2} \\ P &= \eta \frac{1 + 2\sqrt{\alpha - \alpha^2} \cos(\Delta\Phi_U - \Delta\Phi_L)}{2}. \end{aligned} \quad (2.8)$$

In case of $\eta = 1$, $\alpha = 0.5$ and $\Delta\Phi_U = -\Delta\Phi_L = \Delta\Phi$, (2.8) simplifies as

$$P = \frac{1 + \cos(2\Delta\Phi)}{2}.$$

Defining θ as the parasitic phase modulation of the AM signal, it is possible to obtain the instantaneous frequency chirping $\Delta f(t)$ as

$$\Delta f(t) = \frac{1}{2\pi} \tan^{-1} \left[\frac{\alpha \sin(\Delta\Phi_U) + (1-\alpha) \sin(\Delta\Phi_L)}{\alpha \cos(\Delta\Phi_U) + (1-\alpha) \cos(\Delta\Phi_L)} \right]$$

where the time derivative is implemented by an internal component DVDT.

2.5 Implementation

[3]The implementation of the two blocks just described has been realized exploiting the Model Wizard Tool provided by AWR MWOFFICE. The source codes describing the behaviour of the devices are written in C++, then compiled into a Dynamic-Linked Library (DLL) using Microsoft Visual Studio. Once the DLL is installed a library containing all the devices implemented is available in the AWR environment.

Standard base class supplied by AWR are provided in order to describe properly the behaviour of the devices. The one exploited in this particular project are:

- **KNoCacheElectModel** class, in order to provide a description of linear models through their frequency domain admittance matrix;
- **KCacheElectModel** class, in order to provide a description of multiport elements through their $Y - Matrix$;
- **KNoAggregateModel** class, in order to characterize a linear model with an equivalent network using a user defined netlist;
- **KNL3BranchModel** class, in order to provide a description of a generic three-port nonlinear VCCS that has an output current controlled by its three branch voltages.

2.5.1 Phase Modulator Implementation

A Top-Down implementation strategy is exploited to build the Phase Modulation Block. The top level structures are described as an aggregate models of all the bottom level components until the last level is reached i.e. the one that has components which must be described by their Y-matrix, or which have an equivalent circuit made of standard elements.

Once in the working space, a model interface makes it possible for the user to set the following parameters

- $V_\pi L$ [$V \cdot m$] (product between the $ON - OFF$ driving voltage and the length of the active region);
- L [m] (active region length);
- n_o (effective refractive index for the optical field);
- n_m (effective refractive index for the RF field);
- R [Ω/m] (DC substrate/electrode resistance per unit of length);
- α_0 [Np/m] (conductor skin effect attenuation);
- α_1 [Np/m] (dielectric loss attenuation factor);
- f_0 [Hz] (attenuation frequency reference);
- Z_0 [Ω] (line characteristic impedance);
- *PhaseReversal* (flag which alters the sign of V_π).

It has to be noticed that the transmission line complex propagating constant γ_m is computed taking into account both the dielectric and the conductor attenuation factors, the formula adopted in the model is:

$$\gamma_m = \alpha_0 \sqrt{\frac{f}{f_0}} + \alpha_1 \frac{f}{f_0} + j \frac{2\pi}{c_0} n_m f.$$

A further version of the PM block has been developed making it possible to import the frequency-dependent microwave propagation characteristics computed through external EM models as user-defined files of frequency samples. It is exploited when a more accurate analysis is needed or the waveguide structures under test are more complex or unconventional.

2.5.2 Interferometer Implementation

The AM block is a non-linear four port device described by the following equation

$$P_{out} = P_{in} \eta \frac{1 + 2\sqrt{\alpha - \alpha^2} \cos(\Delta\Phi_U(t) - \Delta\Phi_L(t))}{2} \quad (2.9)$$

It is implemented cascading a non linear controlled current source (VCCS) with a network of linear components where the optical quantities are represented by electrical ones. Therefore, (2.9) is represented as:

$$I_{out} = V_{in} \eta \frac{1 + 2\sqrt{\alpha - \alpha^2} \cos(V_{\Delta\phi})}{2} \quad (2.10)$$

where

- $P_{out} \rightarrow I_{out}$;
- $P_{in} \rightarrow V_{in}$;
- $\Delta\Phi_U(t) - \Delta\Phi_L(t) \rightarrow V_{\Delta\phi}$.

and

- η (overall power efficiency $0 \leq \eta \leq 1$);
- α (beam splitter asymmetry factor $0 \leq \alpha \leq 1$);

are the input variable that can be set by the user.

The presence of the linear network is necessary to fulfil three functions:

1. the need to convert the current representing the phase shift of a single arm coming from the PM block into a voltage of the same amplitude (using unitary resistors) to interface it properly with the non-linear controlled current source;

2. the need to compute the phase difference $\Delta\Phi_U(t) - \Delta\Phi_L(t)$;
3. the need to introduce small additional elements used to overcome the restriction that does not allow non linear elements to be connected in parallel. Therefore, the VCCS has not direct access to the external ports, and so the whole component can be freely linked to other non-linear elements.

Chapter 3

Plasmonic Waveguides

3.1 Introduction

Differently from the previous chapters, the analysis moves on the characterization of plasmonic waveguides, these particular structures will be exploited as active areas when the plasmonic electro-optical modulator will be discussed, their main feature is the capability to highly confine the RF electric field at the interface between the metal and the electro-optic material. The chapter starts with a general characterization of the surface plasmons, then the study of the plasmonic waveguide field distribution is carried out, with particular care in the description of the simple propagation at the dielectric-Metal interface and then the propagation in metal-dielectric-metal structures. In particular, it will be demonstrated that this last configuration supports both oscillatory modes (common TE and TM modes) characterized by real propagation constants, and plasmonic modes characterized by imaginary propagation constants, they can propagate as TM waves only in a certain wavelength range, precisely the one corresponding to a negative real part

of the metal permittivity (NIR to visible range).

3.2 Characterization

[6]Surface plasmons or polaritons are waves propagating along the interface between a dielectric material and a metal but attenuating exponentially in both media, they exist when the metal permittivity has a negative real part. In order to introduce a first generic characterization, a basic structure made of three layers is defined thaking as reference Fig.3.1:

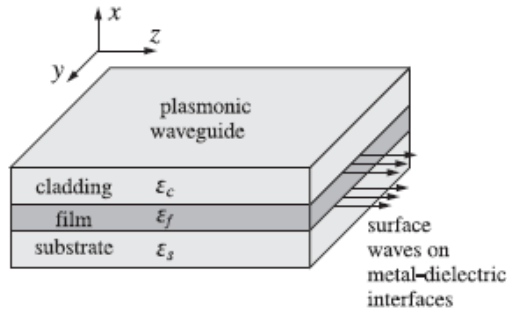


Figure 3.1. [6]Plasmonic Waveguide.

- the *cladding* and *substrate* (characterized respectively by their relative permittivities ϵ_c and ϵ_s) are the two external layers;
- the in-between region is named *film* (characterized by its relative permittivity ϵ_f).

In the following analysis, the two side regions are supposed to have infinite extension along the y -direction while the film is thick $2a$. The propagation takes place in the z -direction while the transverse confinement direction is along x ; the overall field solution has a dependence from time t and the propagation direction z of the kind:

$$e^{j(\omega t - \beta z)}.$$

Starting from the study of the field propagation in the side regions along the x -direction, it can be noticed that the attenuation coefficients real part corresponding to the cladding α_c and substrate α_s have to be positive since the field behaviour is exponentially decaying away from the interface, therefore, the field shape for $x < -a$ (substrate) and $x > a$ (cladding) is:

$$e^{-\alpha_{c,s}|x|}$$

with

$$\begin{aligned}\alpha_s^2 &= \beta^2 - k_0^2 \epsilon_s \\ \alpha_c^2 &= \beta^2 - k_0^2 \epsilon_c\end{aligned}\quad (3.1)$$

where $k_0 = 2\pi/\lambda_0$ is the vacuum wavenumber and λ_0 is the wavelength corresponding to the operating frequency $f_0 = c_0/\lambda_0$.

In the z direction, the solutions (β) that guarantee the exponential attenuation of the electric field while propagating in the z -directions are the ones with negative imaginary parts

$$\beta = \beta_R - j\beta_I \quad \text{with} \quad \beta_I \geq 0. \quad (3.2)$$

and so

$$e^{-j\beta z} = e^{-j(\beta_R - j\beta_I)z} = e^{-j\beta_R z} e^{-\beta_I z}.$$

In the film region, the solutions in the x -direction are a linear combination of hyperbolic terms ($\sinh(\gamma x)$ and $\cosh(\gamma x)$), they are denoted as *Plasmonic Solutions* where γ has been defined as an "attenuation" coefficient. In order to find γ the following relation is imposed

$$k_f^2 = k_0^2 \epsilon_f - \beta^2$$

where k_f is the transverse cutoff wavenumber.

Finally γ is defined as:

$$\gamma^2 = -k_f^2 \quad \text{or} \quad \gamma = jk_f. \quad (3.3)$$

Relation (3.3) holds especially in case the film region is a metal with a negative real part of the dielectric constant (i.e. $k_f^2 < 0$).

In order to find plasmonic solutions (TM mode solutions) the following equations have to be solved in each region:

$$\begin{aligned}\frac{\partial^2 E_z}{\partial x^2} + (k_0^2 \epsilon_i - \beta^2) E_z &= 0 \\ E_x &= -j \frac{\beta}{-\gamma^2} \frac{\partial E_z}{\partial x} \\ H_y &= \frac{\omega \epsilon_0 \epsilon_i}{\beta} E_x\end{aligned}\quad (3.4)$$

where i corresponds to c, f, s . The following field distributions are obtained:

$$H_y(x) = \begin{cases} j\omega\epsilon_0 E_0 \frac{\epsilon_f}{\gamma} \cosh(\gamma x + \psi) & |x| \leq a \\ -j\omega\epsilon_0 E_0 \frac{\epsilon_c}{\alpha_c} \sinh(\gamma a + \psi) e^{-\alpha_c(x-a)} & x \geq a \\ -j\omega\epsilon_0 E_0 \frac{\epsilon_s}{\alpha_s} \sinh(\gamma a - \psi) e^{\alpha_s(x+a)} & x \leq -a \end{cases} \quad (3.5)$$

imposing $E_z = j \frac{1}{\omega\epsilon_0\epsilon_i} \frac{\partial H_y}{\partial x}$ it is possible to obtain $E_z(x)$

$$E_z(x) = \begin{cases} E_0 \sinh(\gamma x + \psi) & |x| \leq a \\ E_0 \sinh(\gamma a + \psi) e^{-\alpha_c(x-a)} & x \geq a \\ E_0 \sinh(\gamma a - \psi) e^{\alpha_s(x+a)} & x \leq -a \end{cases} \quad (3.6)$$

imposing $E_x = -\frac{\beta}{\omega\epsilon_0\epsilon_i} H_y$ it is possible to obtain $E_x(x)$

$$E_x(x) = \begin{cases} E_0 \frac{j\beta}{\gamma} \cosh(\gamma x + \psi) & |x| \leq a \\ -E_0 \frac{j\beta}{\alpha_c} \sinh(\gamma a + \psi) e^{-\alpha_c(x-a)} & x \geq a \\ -E_0 \frac{j\beta}{\alpha_s} \sinh(\gamma a - \psi) e^{\alpha_s(x+a)} & x \leq -a \end{cases} \quad (3.7)$$

It can be noticed that imposing the continuity of the tangential H -field at the interfaces ($x = \pm a$) is equivalent to impose the continuity of the normal D -field (ϵE_x), it results in:

$$\begin{aligned} \frac{\epsilon_f}{\gamma} \cosh(\gamma a + \psi) &= -\frac{\epsilon_c}{\alpha_c} \sinh(\gamma a + \psi) \\ \frac{\epsilon_f}{\gamma} \cosh(\gamma a - \psi) &= -\frac{\epsilon_s}{\alpha_s} \sinh(\gamma a - \psi) \end{aligned}$$

which becomes

$$\begin{aligned} \tanh(\gamma a + \psi) &= -\frac{\rho_c \alpha_c}{\gamma} \\ \tanh(\gamma a - \psi) &= -\frac{\rho_s \alpha_s}{\gamma}. \end{aligned} \quad (3.8)$$

where

$$\rho_c = \frac{\epsilon_f}{\epsilon_c} \quad \text{and} \quad \rho_s = \frac{\epsilon_f}{\epsilon_s} \quad (3.9)$$

Substituting (3.8), the system of solutions (3.5) can be rewritten as

$$H_y(x) = \begin{cases} H_0 \sinh(\gamma x + \psi) & |x| \leq a \\ H_0 \sinh(\gamma a + \psi) e^{-\alpha_c(x-a)} & x \geq a \\ H_0 \sinh(\gamma a - \psi) e^{\alpha_s(x+a)} & x \leq -a \end{cases} \quad (3.10)$$

where

$$H_0 = j\omega\epsilon_0 E_0 \frac{\epsilon_f}{\gamma}.$$

Equations (3.8) can be decoupled in

$$\tanh(2\gamma a) = -\frac{\gamma(\rho_c\alpha_c + \rho_s\alpha_s)}{\gamma^2 + \rho_c\alpha_c\rho_s\alpha_s} \quad (3.11)$$

and

$$\tanh(2\psi) = -\frac{\gamma(\rho_c\alpha_c - \rho_s\alpha_s)}{\gamma^2 - \rho_c\alpha_c\rho_s\alpha_s}. \quad (3.12)$$

It is possible to find β , γ , α_c and α_s (complex quantities when the media are lossy) from (3.11) and from the following expression:

$$\begin{aligned} \gamma^2 &= k_0^2\epsilon_f - \beta^2 \\ \alpha_c^2 &= k_0^2\epsilon_c - \beta^2 \\ \alpha_s^2 &= k_0^2\epsilon_s - \beta^2. \end{aligned} \quad (3.13)$$

Then ψ can be found, it is defined up to an integer multiple of $j\pi/2$ since the following relation holds

$$\tanh(2\psi \pm jm\pi) = \tanh(2\psi)$$

where the introduction of m is necessary to denote particular modes. It is possible to write the inverse of (3.8) as:

$$\gamma a + \psi = \tanh^{-1} \left(-\frac{\rho_c\alpha_c}{\gamma} \right)$$

and

$$\gamma a - \psi = \tanh^{-1} \left(-\frac{\rho_s \alpha_s}{\gamma} \right) - jm\pi$$

leading to

$$\gamma a = \frac{1}{2} \tanh^{-1} \left(-\frac{\rho_c \alpha_c}{\gamma} \right) + \frac{1}{2} \tanh^{-1} \left(-\frac{\rho_s \alpha_s}{\gamma} \right) - \frac{1}{2} jm\pi \quad (3.14)$$

and

$$\psi = \frac{1}{2} \tanh^{-1} \left(-\frac{\rho_c \alpha_c}{\gamma} \right) - \frac{1}{2} \tanh^{-1} \left(-\frac{\rho_s \alpha_s}{\gamma} \right) + \frac{1}{2} jm\pi. \quad (3.15)$$

As it will be discussed, the modes of interest are the TM_0 and TM_1 corresponding to $m = 0$ and $m = 1$. If an additional $j\pi/2$ term is present, depending on the value of the parameter, (3.14) and (3.15) becomes

$$\gamma a = \frac{1}{2} \tanh^{-1} \left(-\frac{\gamma}{\rho_c \alpha_c} \right) + \frac{1}{2} \tanh^{-1} \left(-\frac{\gamma}{\rho_s \alpha_s} \right) - \frac{1}{2} j(m) - 1\pi \quad (3.16)$$

$$\psi = \frac{1}{2} \tanh^{-1} \left(-\frac{\gamma}{\rho_c \alpha_c} \right) - \frac{1}{2} \tanh^{-1} \left(-\frac{\gamma}{\rho_s \alpha_s} \right) + \frac{1}{2} jm\pi \quad (3.17)$$

where the following relation has been used

$$\tanh^{-1}(x) = \tanh^{-1} \left(\frac{1}{x} \right) + \text{sign}(x)j\frac{\pi}{2}$$

valid for x real and $|x| < 1$.

It can be noticed that (3.12) is equal to zero in case of a symmetric structure (i.e. $\epsilon_c = \epsilon_s$ and $\alpha_c = \alpha_s$) leading to two possible solutions $\psi = 0$ and $\psi = j(\pi/2)$. The first solution is denoted as *even* or *symmetric* due to the fact that the corresponding transverse electric field $E_x(x)$ and magnetic field $H_y(x)$ are symmetric within the film region (they are proportional to $\cosh(\gamma x)$ which is an even function of x). In case of even modes, (3.11) becomes:

$$\tanh(\gamma a) = -\frac{\rho_c \alpha_c}{\gamma}. \quad (3.18)$$

The second solution is instead denoted as *odd* or *antisymmetric* due to the antisymmetry of the transverse electric field $E_x(x)$ and magnetic field $H_y(x)$ that are proportional to $\cosh(\gamma x + j\pi/2) = j \sinh(\gamma x)$ odd function of x . In the odd case equation (3.11) becomes:

$$\coth(\gamma a) = -\frac{\rho_c \alpha_c}{\gamma} \quad (3.19)$$

where the identity

$$\tanh\left(x \pm j\frac{\pi}{2}\right) = \coth(x)$$

has been exploited.

The notation *even/symmetric* and *odd/antisymmetric* also holds for non symmetric structures, corresponding respectively to solutions that have value of ψ mostly real (even) or with imaginary part close to $j\pi/2$ (odd).

3.2.1 Oscillatory Modes

Plasmonic waveguides support not only plasmonic modes but also oscillatory ones, where the peak of the field instead of being at the interfaces is at the centre of the film region (as happens in common waveguides). In this case the waves are characterized by $\gamma = jk_f$ which is predominantly imaginary, k_f is defined as:

$$k_f = \sqrt{k_0^2 \epsilon_f - \beta^2}.$$

Substituting jk_f it in (3.11), the result is:

$$\tanh(2k_f a) = \frac{k_f(\rho_c \alpha_c + \rho_s \alpha_s)}{k_f^2 + \rho_c \alpha_c \rho_s \alpha_s} \quad (3.20)$$

where the identity

$$\tanh(jx) = j \tanh(x)$$

has been exploited.

If k_f is predominantly real, both TE and TM modes exist and the TE solutions are the ones obtained setting $\rho_c = \rho_s = 1$. Imposing $\psi = j\phi$, (3.8) becomes:

$$\begin{aligned} \tanh(k_f a + \phi) &= -\frac{\rho_c \alpha_c}{k_f} \\ \tanh(k_f a - \phi) &= -\frac{\rho_s \alpha_s}{k_f} \end{aligned} \quad (3.21)$$

while (3.14) and (3.15) become:

$$k_f a = \frac{1}{2} \tanh^{-1}\left(\frac{\rho_c \alpha_c}{k_f}\right) + \frac{1}{2} \tanh^{-1}\left(-\frac{\rho_s \alpha_s}{k_f}\right) + \frac{1}{2} m\pi \quad (3.22)$$

and

$$\psi = \frac{1}{2} \tanh^{-1} \left(-\frac{\rho_c \alpha_c}{k_f} \right) - \frac{1}{2} \operatorname{atanh} \left(-\frac{\rho_s \alpha_s}{k_f} \right) + \frac{1}{2} m\pi \quad (3.23)$$

that are valid both for TE and TM modes.

In the following sections, the procedure just described will be applied in order to find the plasmonic solutions for the simple case of propagation in a single *Dielectric-Metal* interface and in case of propagation in a *Metal-Dielectric-Metal* structure.

3.3 Metal-Dielectric Interface

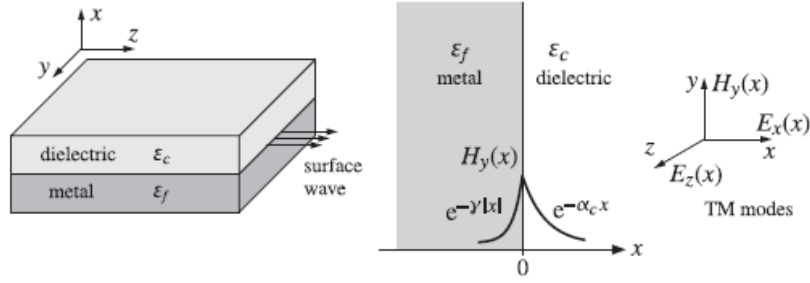


Figure 3.2. [6] Metal Dielectric Structure.

[6]As it can be seen in Fig.3.2, the guiding structure is composed of two semi-infinite section, the metal film (where a has been considered infinite) and the dielectric cladding, with the interface placed at $x = 0$.

Considering a dependency from the propagation direction z and from time t of the kind

$$e^{j\omega t - \beta z}$$

the field components for TM modes can be obtained from (3.4) as:

$$H_y(x) = \begin{cases} -j\omega\epsilon_0 E_0 \frac{\epsilon_d}{\alpha_d} e^{-\alpha_d x} & x \geq 0 \\ j\omega\epsilon_0 E_0 \frac{\epsilon_m}{\gamma} e^{-\gamma|x|} & x \leq 0 \end{cases} \quad (3.24)$$

$$E_x(x) = \begin{cases} -E_0 \frac{j\beta}{\alpha_d} e^{-\alpha_d x} & x \geq 0 \\ E_0 \frac{j\beta}{\gamma} e^{-\gamma|x|} & x \leq 0 \end{cases} \quad (3.25)$$

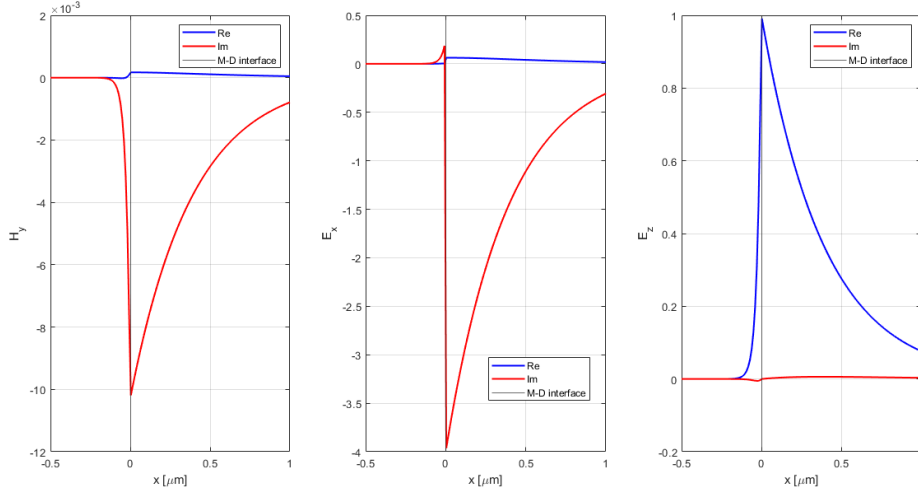


Figure 3.3. Field Components for TM modes.

$$E_z(x) = \begin{cases} E_0 e^{-\alpha_d x} & x \geq 0 \\ E_0 e^{-\gamma|x|} & x \leq 0 \end{cases} \quad (3.26)$$

where the subscript m and d respectively identify the metal and the dielectric. Due to the continuity of the transverse component of the magnetic field (H_y) at the interface ($x = 0$) the following condition is obtained:

$$\gamma = -\epsilon_m \frac{\alpha_d}{\epsilon_d} \quad (3.27)$$

leading to

$$\beta^2 - k_0^2 \epsilon_m = \frac{\epsilon_m^2}{\epsilon_d^2} = (\beta^2 - k_0^2 \epsilon_d).$$

Equation (3.27) can be solved in order to find β , γ and α_d , the results are:

$$\beta = k_0 \sqrt{\frac{\epsilon_m \epsilon_d}{\epsilon_m + \epsilon_d}} \quad (3.28)$$

$$\gamma = -\frac{k_0 \epsilon_m}{\sqrt{-\epsilon_m - \epsilon_d}} \quad (3.29)$$

$$\alpha_d = \frac{k_0 \epsilon_d}{\sqrt{-\epsilon_m - \epsilon_d}} \quad (3.30)$$

where the imaginary part of β (β_I) is negative and the real part of β (β_R), α_d and γ are positive. Defining

$$\epsilon_m = -\epsilon_R - j\epsilon_I$$

it is possible to rewrite (3.28), (3.30) and (3.29) as follows:

$$\beta = k_0 \sqrt{\frac{\epsilon_R \epsilon_d}{\epsilon_R - \epsilon_d}} \left[1 - j \frac{\epsilon_I \epsilon_d}{2\epsilon_R(\epsilon_R - \epsilon_d)} \right] \quad (3.31)$$

$$\gamma = \frac{k_0 \epsilon_R}{\sqrt{\epsilon_R - \epsilon_d}} \left[1 + j \frac{\epsilon_I(\epsilon_R - 2\epsilon_d)}{2\epsilon_R(\epsilon_R - \epsilon_d)} \right] \quad (3.32)$$

$$\alpha_d = \frac{k_0 \epsilon_d}{\sqrt{\epsilon_R - \epsilon_d}} \left[1 - j \frac{\epsilon_I}{2(\epsilon_R - \epsilon_d)} \right] \quad (3.33)$$

which shows that in order to have $\beta_R > 0$ and $\beta_I < 0$ and to guarantee the existence of plasmonic waves it is necessary to have $\epsilon_R > \epsilon_d$. Considering $\epsilon_R \gg \epsilon_d$, from (3.33) and (3.32) it results:

$$\frac{Re(\gamma)}{Re(\alpha_d)} = \frac{\epsilon_R}{\epsilon_d} \gg 1$$

therefore

$$\frac{1}{Re(\gamma)} \ll \frac{1}{Re(\alpha_d)} \quad (3.34)$$

where $1/Re(\gamma)$ and $1/Re(\alpha_d)$ are the attenuation lengths. Equation (3.34) highlights that the field penetrates more in the dielectric than in the metal since the attenuation length within the metal is shorter.

3.4 Metal-Dielectric-Metal waveguide

[6] In this section the propagation through the MDM structure is analysed taking into account the lossless case for sake of simplicity.

3.4.1 Lossless Media

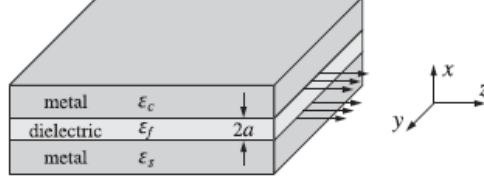


Figure 3.4. [6]Field Components for TM modes.

The structure under analysis is made of three region, a dielectric lossless film characterized by ϵ_f real and positive and metal substrate and cladding respectively characterized by ϵ_s and ϵ_c real and negative. Defining $\epsilon_s = -|\epsilon_s|$ and $\epsilon_c = -|\epsilon_c|$ with $|\epsilon_s| \leq |\epsilon_c|$, there are three possible working regions:

1. $|\epsilon_s| \leq \epsilon_f \leq |\epsilon_c|$;
2. $|\epsilon_s| \leq |\epsilon_c| \leq \epsilon_f$;
3. $\epsilon_f \leq |\epsilon_s| \leq |\epsilon_c|$;

where the region of interest for typical metals at optical frequency is the third.

In the MDM configuration, (3.8) and (3.11) become:

$$\tanh(\gamma a + \psi) = -\frac{\rho_c \alpha_c}{\gamma} = \frac{|\rho_c| \alpha_c}{\gamma} \quad (3.35)$$

$$\tanh(\gamma a - \psi) = -\frac{\rho_s \alpha_s}{\gamma} = \frac{|\rho_s| \alpha_s}{\gamma}.$$

$$\tanh(2\gamma a) = -\frac{\gamma(\rho_c \alpha_c + \rho_s \alpha_s)}{\gamma^2 + \rho_c \alpha_c \rho_s \alpha_s} = \frac{\gamma(|\rho_c| \alpha_c + |\rho_s| \alpha_s)}{\gamma^2 + |\rho_c| \alpha_c |\rho_s| \alpha_s} \quad (3.36)$$

while β , α_c and α_s can be rewritten as:

$$\gamma = \sqrt{\beta^2 - k_0^2 \epsilon_f}$$

$$\alpha_c = \sqrt{\beta^2 - k_0^2 \epsilon_c} = \sqrt{\gamma^2 + k_0^2 (\epsilon_f + |\epsilon_c|)}. \quad (3.37)$$

$$\alpha_s = \sqrt{\beta^2 - k_0^2 \epsilon_s} = \sqrt{\gamma^2 + k_0^2 (\epsilon_f + |\epsilon_s|)}$$

where $\beta \geq k_0 \sqrt{\epsilon_f}$ and $\gamma \geq 0$ to allow the existence of plasmonic solutions.

From (3.36) it is possible to find the cutoff thickness of the dielectric a_{cutoff} taking the limit as $\gamma \rightarrow 0$. In this case it is possible to exploit the Taylor series approximation:

$$\tanh(x) \approx x \quad x \rightarrow 0;$$

therefore

$$\tanh(2\gamma a) \approx 2\gamma a = -\frac{\gamma(\rho_c \alpha_c + \rho_s \alpha_s)}{\gamma^2 + \rho_c \alpha_c \rho_s \alpha_s} = \frac{\gamma(|\rho_c| \alpha_c + |\rho_s| \alpha_s)}{\gamma^2 + |\rho_c| \alpha_c |\rho_s| \alpha_s} \quad (3.38)$$

$$2a = \frac{1}{|\rho_c| \alpha_c} + \frac{1}{|\rho_s| \alpha_s}$$

when $\gamma = 0$

$$2k_0 a_{\text{cutoff}} = \frac{|\epsilon_c|}{\epsilon_f \sqrt{\epsilon_f + |\epsilon_c|}} + \frac{|\epsilon_s|}{\epsilon_f \sqrt{\epsilon_f + |\epsilon_s|}}. \quad (3.39)$$

Region 1 is defined by

$$|\epsilon_s| \leq \epsilon_f \leq |\epsilon_c| \quad (3.40)$$

leading to

$$\alpha_s > \gamma$$

and

$$\frac{|\rho_s| \alpha_s}{\gamma} \geq 1$$

therefore

$$\tanh(\gamma a - \psi) = \frac{|\rho_s| \alpha_s}{\gamma} \geq 1$$

where $\psi = \chi + j\frac{\pi}{2}$ with real χ . Substituting in the previous equation

$$\tanh(\gamma a - \psi) = \tanh\left(\gamma a - \chi - j\frac{\pi}{2}\right) = \coth(\gamma a - \chi) = \frac{|\rho_s| \alpha_s}{\gamma} \geq 1.$$

It can be demonstrated that also $\frac{|\rho_c| \alpha_c}{\gamma} \geq 1$ holds because:

$$\tanh(\gamma a + \psi) = \tanh\left(\gamma a + \chi + j\frac{\pi}{2}\right) = \coth(\gamma a + \chi) = \frac{|\rho_c| \alpha_c}{\gamma}.$$

If γ and χ are real

$$|\coth(\gamma a + \chi)| = \frac{|\rho_c| \alpha_c}{\gamma} \geq 1.$$

Not all the values of beta satisfy the previous expression that imposes an upper limit on β

$$\gamma^2 \leq |\rho_c|^2 \alpha_c^2$$

substituting (3.37)

$$\beta^2 - k_0^2 \epsilon_f \leq \rho_c^2 (\beta^2 - k_0^2 |\epsilon_c|)$$

$$\beta^2 \leq k_0^2 \frac{\rho_c^2 |\epsilon_c| + \epsilon_f}{1 - \rho_c^2} = k_0^2 \frac{|\epsilon_c| \epsilon_f}{|\epsilon_c| - \epsilon_f}$$

$$\beta \leq k_0 \sqrt{\frac{|\epsilon_c| \epsilon_f}{|\epsilon_c| - \epsilon_f}} = k_0 \sqrt{\frac{\epsilon_c \epsilon_f}{\epsilon_c - \epsilon_f}} \equiv \beta_{c,\infty}$$

therefore the range of β in region 1 is

$$k_0 \epsilon_f \leq \beta \leq \beta_{c,\infty}.$$

The thickness of the film region a results to be an increasing function of beta with

$$a_{\text{cutoff}} \leq a < \infty$$

where a_{cutoff} is a lower cutoff. As $a \rightarrow \infty$, the structure tends to the one studied in the case of a single interface and the magnetic field tends to be more confined at the *film-cladding* interface. Plasmonic solutions are found at the interface between *film* and *cladding* since the condition $|\epsilon_m| \leq \epsilon_d$ at the *film-substrate* interface does not allow their existence. To find γa and ψ the starting point is:

$$\coth(\gamma a + \chi) = \frac{|\rho_c| \alpha_c}{\gamma} \tag{3.41}$$

$$\coth(\gamma a - \chi) = \frac{|\rho_s| \alpha_s}{\gamma}. \tag{3.42}$$

Inverting the last two equations, the following expression are obtained:

$$\tanh(\gamma a + \chi) = \frac{\gamma}{|\rho_c| \alpha_c} \leq 1 \tag{3.43}$$

$$\gamma a + \chi = \tanh^{-1} \left(\frac{\gamma}{|\rho_c| \alpha_c} \right) \tag{3.44}$$

and

$$\tanh(\gamma a - \chi) = \frac{\gamma}{|\rho_s|\alpha_s} \leq 1 \quad (3.45)$$

$$\gamma a - \chi = \tanh^{-1}\left(\frac{\gamma}{|\rho_s|\alpha_s}\right). \quad (3.46)$$

Finally

$$\gamma a = \frac{1}{2} \tanh^{-1}\left(\frac{\gamma}{|\rho_c|\alpha_c}\right) + \frac{1}{2} \tanh^{-1}\left(\frac{\gamma}{|\rho_s|\alpha_s}\right) \quad (3.47)$$

$$2\psi = \frac{1}{2} \tanh^{-1}\left(\frac{\gamma}{|\rho_c|\alpha_c}\right) - \frac{1}{2} \tanh^{-1}\left(\frac{\gamma}{|\rho_s|\alpha_s}\right) + j\frac{\pi}{2}. \quad (3.48)$$

The propagating modes are the TM_1 ones (i.e. antisymmetric-like), in this case the magnetic field results to be:

$$H_y(x) = \begin{cases} H_0 \cosh(\gamma x + \psi) & |x| \leq a \\ H_0 \cosh(\gamma a + \psi) e^{-\alpha_c(x-a)} & x \geq a \\ H_0 \cosh(\gamma a - \psi) e^{\alpha_s(x+a)} & x \leq -a \end{cases} \quad (3.49)$$

For small values of χ it results

$$\cosh(\gamma a + \psi) = \cosh\left(\gamma a + \chi + j\frac{\pi}{2}\right) = j \sinh(\gamma a + \chi)$$

that is an odd function of x (i.e. the mode is antisymmetric-like).

Region 2 is characterized by:

$$|\epsilon_s| \leq \epsilon_f \leq |\epsilon_c|. \quad (3.50)$$

In this case

$$k_0 \sqrt{\epsilon_f} \leq \beta \leq \infty \quad (3.51)$$

and

$$0 \leq a \leq a_{\text{cutoff}} \quad (3.52)$$

where a is a decreasing function of β . In this region separate surface plasmons cannot exist at the two interfaces since the condition for their existence is not satisfied ($|\epsilon_m| > \epsilon_d$).

The third region is the one of interest for the desired applications (i.e. the development of a plasmonic electro-optical modulator). It is characterized by

$$\epsilon_f \leq |\epsilon_s| \leq |\epsilon_c| \quad (3.53)$$

and it is the only region that guarantees the existence of the two plasmonic modes (the symmetric-like TM_0 and the antisymmetric-like TM_1) at both interfaces since the condition to have real values of β is satisfied (i.e. $|\epsilon_m| \geq \epsilon_d$), moreover also TE and TM oscillatory modes propagate.

The two interfaces can support separate surface plasmons since $|\epsilon_{c,s}| \geq \epsilon_f$ holds when $a \rightarrow \infty$ (limit of infinite thickness), the corresponding wavenumbers are:

$$\beta_{c,\infty} = \sqrt{\frac{\epsilon_c \epsilon_f}{\epsilon_c + \epsilon_f}} \quad \text{and} \quad \beta_{s,\infty} = \sqrt{\frac{\epsilon_s \epsilon_f}{\epsilon_s + \epsilon_f}} \quad (3.54)$$

where

$$k_0 \sqrt{\epsilon_f} < \beta_{c,\infty} \leq \beta_{s,\infty}. \quad (3.55)$$

The condition (3.53) implies that both the ratios

$$\frac{|\rho_c| \alpha_c}{\gamma} \quad \text{and} \quad \frac{|\rho_s| \alpha_s}{\gamma}$$

can be greater or lower than one, corresponding respectively to the TM_1 mode and the TM_0 . If

$$|\rho_{c,s}| \alpha_{c,s} \leq \gamma$$

and considering

$$\begin{aligned} \rho_c^2 \alpha_c^2 - \gamma^2 &= (1 - \rho_c^2)(\beta_c^2 - \beta^2) \\ \rho_s^2 \alpha_s^2 - \gamma^2 &= (1 - \rho_s^2)(\beta_s^2 - \beta^2) \end{aligned} \quad (3.56)$$

it is possible to obtain the range of β_s for the TM_0 plasmonic mode

$$\beta_{s,\infty} \leq \beta < \infty \quad (3.57)$$

and

$$0 \leq a \leq \infty \quad (3.58)$$

where a is a decreasing function of β , therefore, $\beta = \beta_{s,\infty}$ corresponds to $a = \infty$. If

$$|\rho_{c,s}| \alpha_{c,s} \geq \gamma$$

and considering the (3.56), it is possible to obtain the range of β_s for the TM_1 plasmonic mode:

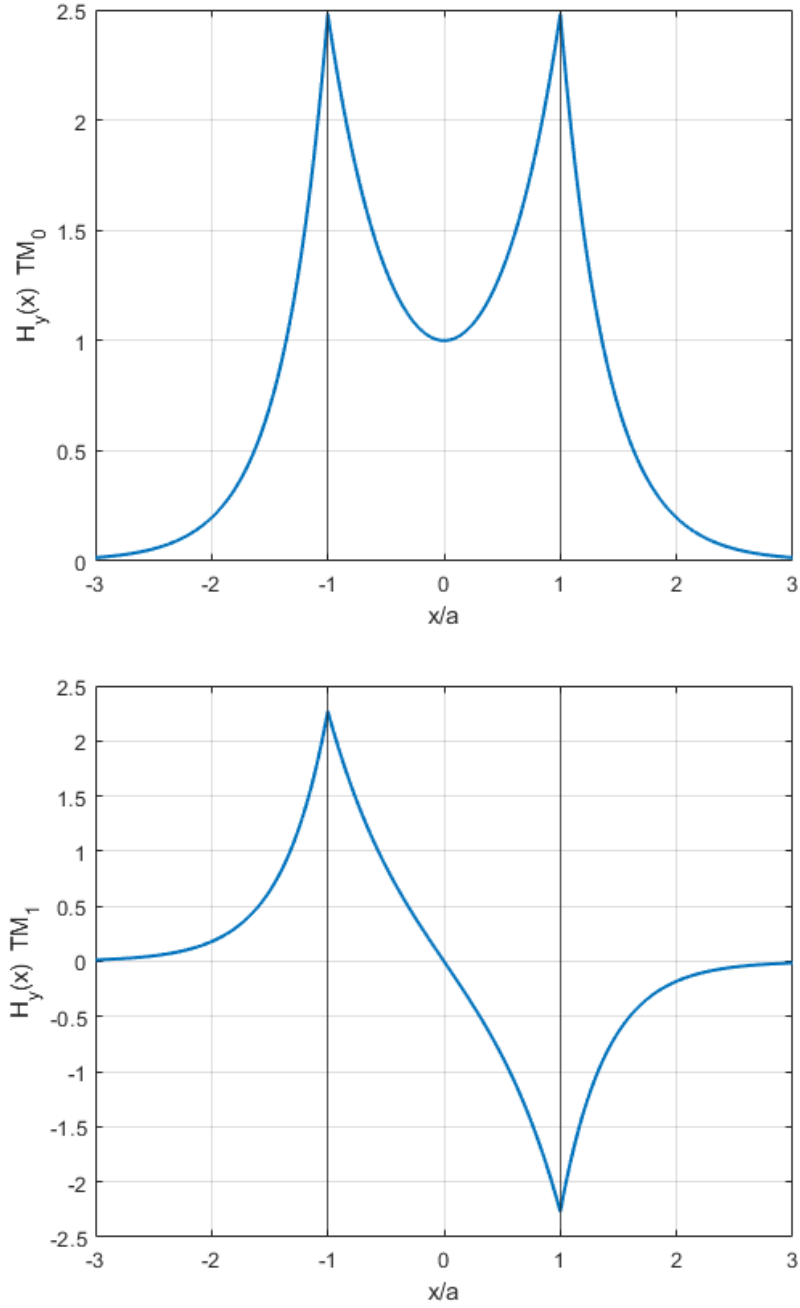


Figure 3.5. $H_y(x)$ field component for the propagating modes.

$$k_0\sqrt{\epsilon_f} \leq \beta < \beta_{c,\infty} \quad (3.59)$$

and

$$a_{\text{cutoff}} \leq a \leq \infty \quad (3.60)$$

is an increasing function of β , therefore, $\beta = \beta_{c,\infty}$ corresponds to $a = \infty$ and $\beta = k_0\sqrt{\epsilon_f}$ corresponds to $a = a_{\text{cutoff}}$.

Equations (3.47) and (3.48) hold for the TM_1 case instead, inverting the following equations, it is possible to obtain γa and ψ for the TM_0 mode

$$\tanh(\gamma a + \psi) = \frac{|\rho_c|\alpha_c}{\gamma} \leq 1 \quad (3.61)$$

$$\tanh(\gamma a - \psi) = \frac{|\rho_s|\alpha_s}{\gamma} \leq 1. \quad (3.62)$$

The results are:

$$\gamma a = \frac{1}{2} \tanh^{-1} \left(\frac{-|\rho_c|\alpha_c}{\gamma} \right) + \frac{1}{2} \tanh^{-1} \left(\frac{-|\rho_s|\alpha_s}{\gamma} \right) \quad (3.63)$$

$$2\psi = \frac{1}{2} \tanh^{-1} \left(\frac{-|\rho_c|\alpha_c}{\gamma} \right) - \frac{1}{2} \tanh^{-1} \left(\frac{-|\rho_s|\alpha_s}{\gamma} \right). \quad (3.64)$$

For imaginary values of γ oscillatory TE and TM modes propagate, where

$$\gamma = jk_f$$

and

$$k_f = \sqrt{k_0^2\epsilon_f - \beta^2}.$$

In order to have γ imaginary and so k_f real, the condition $\beta \leq k_0\sqrt{\epsilon_f}$ has to be satisfied, it imposes an upper limit to the possible values of β . The lower limit of β is imposed by the positivity of α_c and α_s but in this case since $\epsilon_{c,s} < 0$

$$\alpha_{c,s} = \sqrt{\beta^2 - k_0^2\epsilon_{c,s}} = \sqrt{\beta^2 + k_0^2|\epsilon_{c,s}|}$$

the only requirement is that $\beta \geq 0$ and so the range of β is

$$0 \leq \beta \leq k_0\sqrt{\epsilon_f}. \quad (3.65)$$

To find the TE_m modes, ρ_c and ρ_s are set equal to 1 in (3.22) and (3.23), the resulting equations are:

$$k_f a = \frac{1}{2} \tan^{-1} \left(\frac{\alpha_c}{k_f} \right) + \frac{1}{2} \tan^{-1} \left(\frac{\alpha_s}{k_f} \right) + \frac{1}{2} m \pi \quad (3.66)$$

$$2\psi = \frac{1}{2} \tan^{-1} \left(\frac{\alpha_c}{k_f} \right) - \frac{1}{2} \tan^{-1} \left(\frac{\alpha_s}{k_f} \right) + \frac{1}{2} m \pi. \quad (3.67)$$

where $m = 0, 1, 2, 3, \dots$

The TM_m modes are characterized by negative values of ρ_c and ρ_s , therefore the identity

$$\tan^{-1}(x) = \frac{\pi}{2} + \tan^{-1} \left(-\frac{1}{x} \right), \quad x > 0$$

can be applied to rewrite (3.22) and (3.23) in the form:

$$k_f a = \frac{1}{2} \tan^{-1} \left(-\frac{k_f}{\rho_c \alpha_c} \right) + \frac{1}{2} \tan^{-1} \left(-\frac{k_f}{\rho_s \alpha_s} \right) + \frac{1}{2} (m-1) \pi \quad (3.68)$$

and

$$\psi = \frac{1}{2} \tan^{-1} \left(-\frac{k_f}{\rho_c \alpha_c} \right) - \frac{1}{2} \tan^{-1} \left(-\frac{k_f}{\rho_s \alpha_s} \right) + \frac{1}{2} m \pi. \quad (3.69)$$

It is possible to find the lower limit for the thickness of the film region (lower cutoff thickness a_{min}) imposing the condition $\beta = 0$ in (3.66) and (3.68), where $k_f = k_0 \sqrt{\epsilon_f}$ and $\alpha_{c,s} = k_0 \sqrt{-\epsilon_{c,s}}$. The final expressions are:

$$2k_0 a_{min} = \frac{1}{\sqrt{\epsilon_f}} \left[\tan^{-1} \sqrt{\frac{-\epsilon_c}{\epsilon_f}} + \tan^{-1} \sqrt{\frac{-\epsilon_s}{\epsilon_f}} + m \pi \right] \quad (3.70)$$

for the TE_m modes and

$$2k_0 a_{min} = \frac{1}{\sqrt{\epsilon_f}} \left[\tan^{-1} \sqrt{\frac{-\epsilon_c}{\epsilon_f}} + \tan^{-1} \sqrt{\frac{-\epsilon_s}{\epsilon_f}} + (m-1) \pi \right] \quad (3.71)$$

for the TM_m modes. The only oscillatory mode that has an upper cutoff thickness (a_{max}) is the TM_1 . Setting $\beta = k_0 \sqrt{\epsilon_f}$ and so $\alpha_{c,s} = k_0 \sqrt{\epsilon_f - \epsilon_{c,s}}$ a_{max} , the resulting expression is:

$$a_{max} = -\frac{1}{2k_0} \left[\frac{1}{\rho_c \sqrt{\epsilon_f - \epsilon_c}} + \frac{1}{\rho_s \sqrt{\epsilon_f - \epsilon_s}} \right] \quad (3.72)$$

The peculiarity is that a_{max} is the upper cutoff limit for the oscillatory TM_1 mode which exist for $0 \leq \beta \leq k_0 \sqrt{\epsilon_f}$ but, at the same time, it is the lower cutoff limit for the plasmonic TM_1 mode which exist for $k_0 \sqrt{\epsilon_f} \leq \beta \leq \beta_{c,\infty}$.

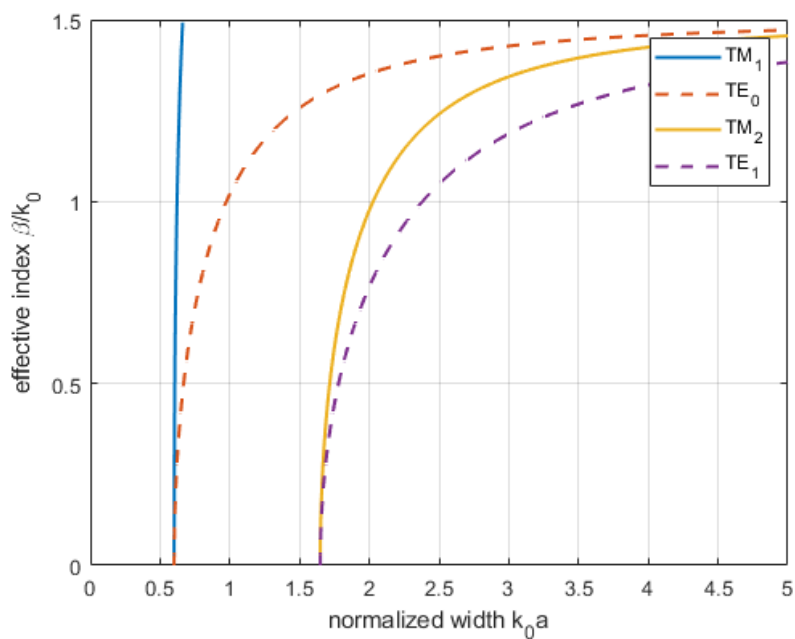


Figure 3.6. effective index for the oscillatory TE and TM modes

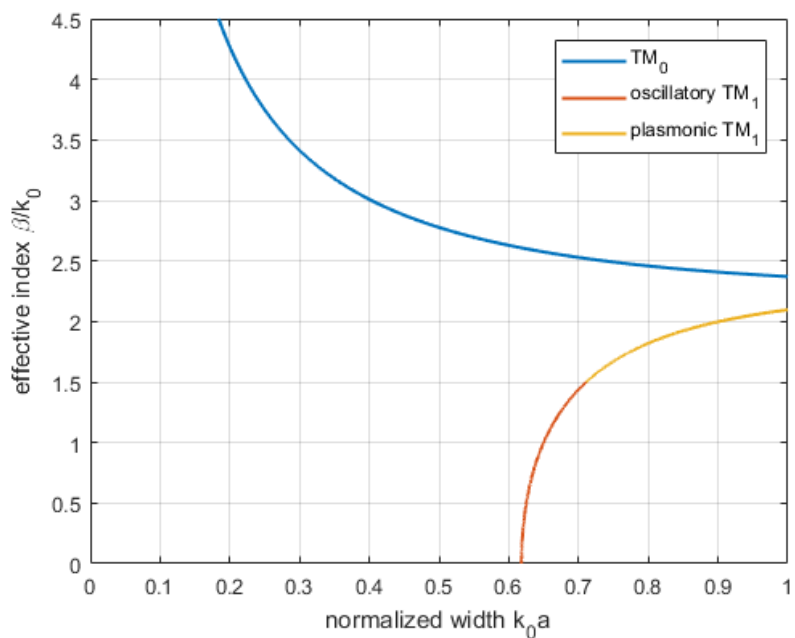


Figure 3.7. effective index TM_0 and TM_1 plasmonic and modes and for the TM_1 oscillatory one.

Chapter 4

EO Plasmonic Mach-Zehnder modulator

4.1 Introduction

In this final chapter the EO Plasmonic Mach-Zehnder modulator is introduced exploiting all the knowledge presented in the previous chapters. These devices represent a valid alternative to LiNbO₃ modulators when the need of very small dimensions has to be accomplished. The small footprint is a key feature that allows to have acceptable losses even though metal layers are present, its cost is the heavy influence of electrical parasitics (strongly layout and realization dependent) on the frequency response. The main characteristics are the possibility to have high speed operation with low power consumption, large electro-optic bandwidth (ideally >100 GHz) and a small voltage-length product. The chapter starts with a preliminary description of the device under analysis then the simulation results obtained combining the characteristic of plasmonic structures and the model developed in the CAD environment are proposed.

4.2 POH Modulator

It is possible to design a Mach-Zehnder modulator using plasmonic interferometers as phase modulator sections, in particular plasmonic-organic hybrid phase shifters are employed. These devices are composed of two MIM (metal-insulator-metal) slot waveguides fabricated on standard SOI wafer (POH structure) where the RF signal is applied at the central electrode through the use of a suspended bridge. The structure is filled with a second order nonlinear optical material (NLO) DLD-164 characterized by linear electro-optic effect (Pockels effect) [7][8][9].

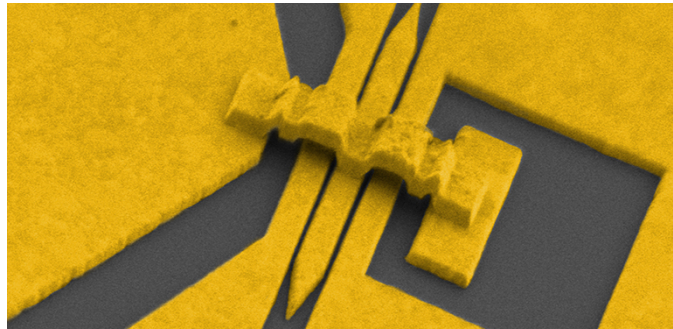


Figure 4.1. [7]Plasmonic Mach-Zehnder Modulator.

As discussed in Ch.3, light propagates as surface plasmons at the metal-insulator interface, the signal is applied at the central electrode inducing between the "island" and the ground electrodes a voltage drop that controls the output phase of the surface plasmons. When the difference between the phase of two arms is π , the modulator is in the off state and the anti-symmetric mode is excited at the output of the phase shifting arms, when it is 0 (i.e. opposite voltage drop is induced) the symmetric one is instead excited.

Many are the advantages offered by the use of NLO materials:

- ultrafast speed (since the only limitation on the electro-optical bandwidth is induced by the RC time constant due to the electrodes and their wires);
- incredibly high value of the r coefficient (increased non linear interaction) which defines the strength of the light-matter interaction and leads to reduced Voltage-lengths products;
- low energy consumption due to the low permittivity at radio frequency and so the reduced capacitance.

In particular, in POH structures, the propagation of surface plasmons at the gold-NLO interface makes possible to achieve additional benefits:

- reduced dimension (few $\sim \mu m^2$) without bandwidth restrictions ($BW > 100$ GHz);
- subdiffraction confinement of light due to the high confinement possible at the metal-insulator interface;
- enhanced light-matter interaction which makes possible to design devices with dimension of the order of micrometers;
- even smaller RC constants thanks to the use of highly conductive metal as electrodes;
- reduced plasmonic losses due to the low plasmonic losses of noble metals;
- possibility to implement stacked modulators (e.g. compact IQ modulators) employing POH modulator due to their small footprint.

Even though other technologies have been investigated as optical modulator, these properties make plasmonic modulators an appealing alternative to LiNbO_3 modulators when small compact devices are required.

4.3 Implementation Details

The behaviour of a Mach-Zehnder POH modulator has been simulated in AWR MWOFFICE exploiting the model described in Ch.2 but, instead of using the common phase modulator block, a version that gives the possibility to describe the device behaviour through frequency varying parameters has been used. In particular it is possible to import a txt file in the project that contains the required data cascaded in the following order:

- frequency [Hz];
- real part of the characteristic impedance [Ω];
- imaginary part of the characteristic impedance [Ω];
- microwave loss [dB/cm];
- microwave effective index;
- optical effective index.

These quantities have been evaluated for a structure where the thickness of the electrodes is $h_{Au} = 22$ nm, the width of the "island" is $W_{island} = 410$ nm, the width of the ground electrodes is $W_{slot} = 100$ nm, the spacing between the electrodes is

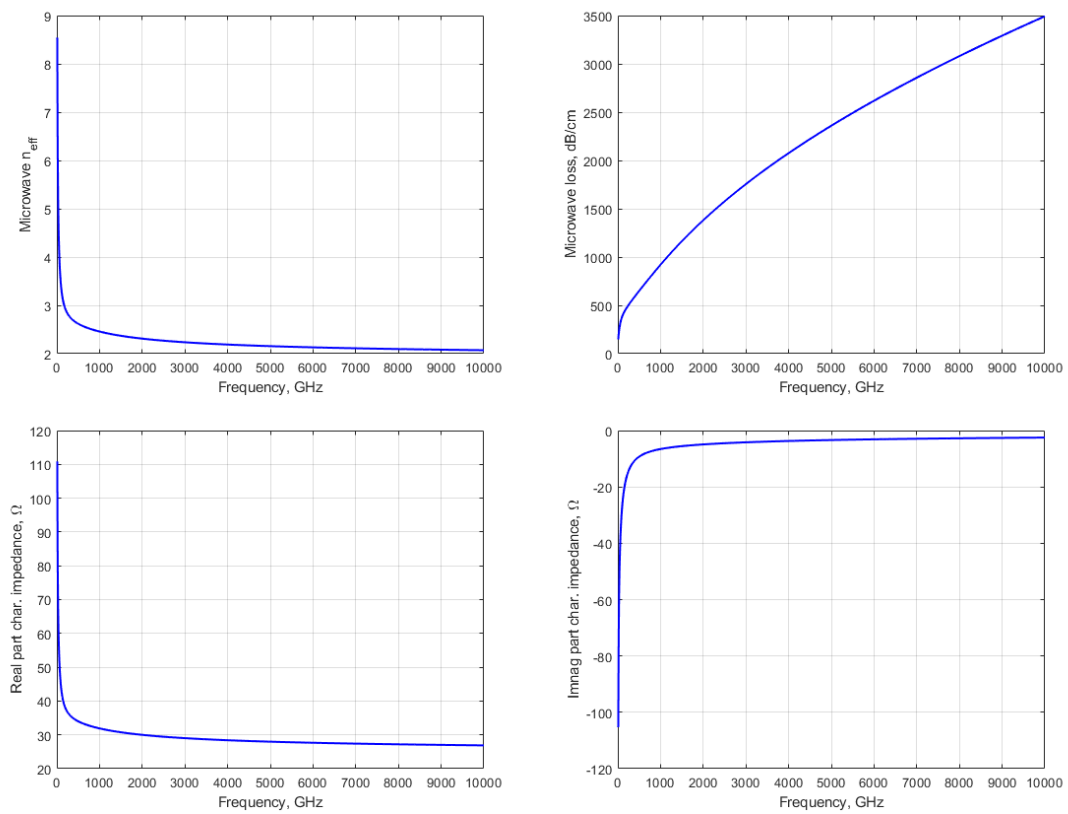


Figure 4.2. RF Effective Refractive Index, Loss, Real and Imaginary Characteristic Impedance.

$W_{rail} = 520$ nm, the dielectric layer is $h_{\text{DLD-164}} = 22$ nm thick and the substrate thickness is $h_{\text{SiO}_2} = 3 \mu\text{m}$ [9].

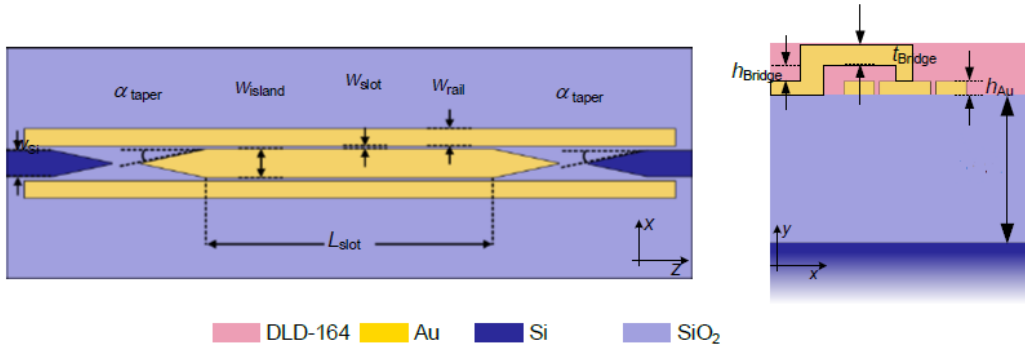


Figure 4.3. [9] Plasmonic Mach-Zehnder Modulator: reference structure.

Concerning the physical characteristics, the DLD-164 has an electro-optic linear coefficient estimated $r_{33} = 180$ pm/V and a refractive index $n = 1.83$, in order to evaluate the permittivity and so the refractive index at the desired frequency, the dispersive nature of the SiO_2 substrate is described by the model from Malitson (Fig. 4.5), while the dispersive nature of gold is described by the Drude model (Fig.4.4).

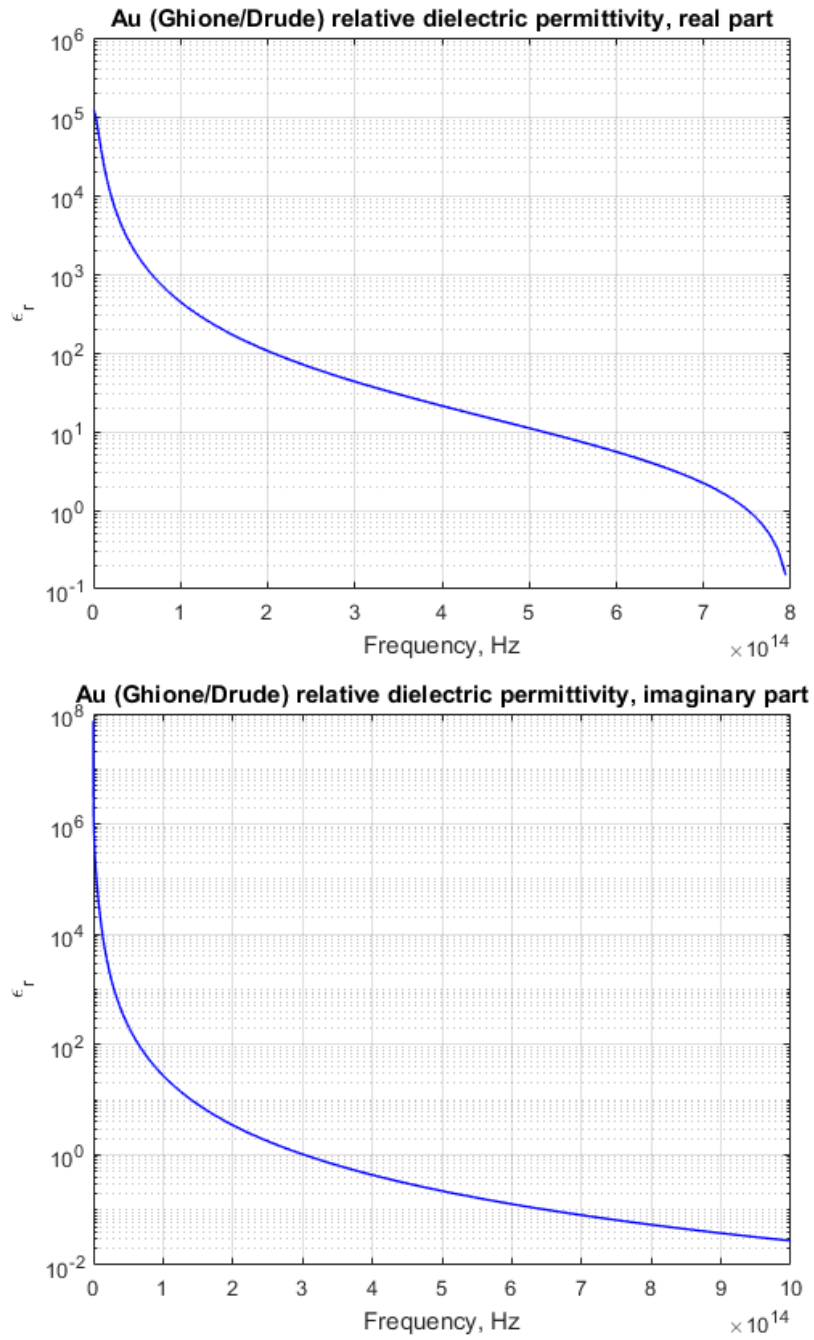


Figure 4.4. Real and Imaginary Permittivity of Gold.

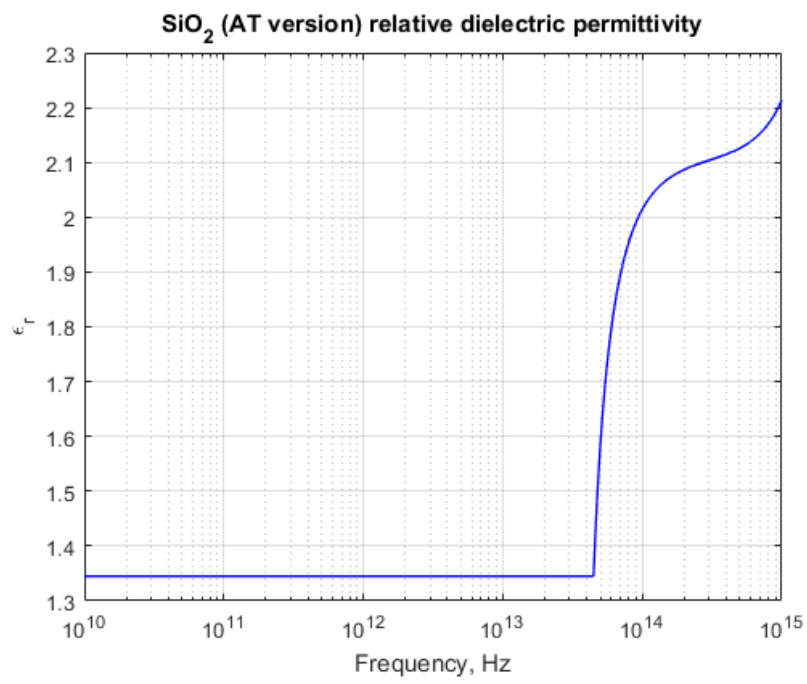


Figure 4.5. Dielectric Permittivity of SiO₂.

As starting point, the phase at the output of the phase shifting arm with respect to a variation of the frequency was obtained. The reference circuit is shown in Fig. 4.6

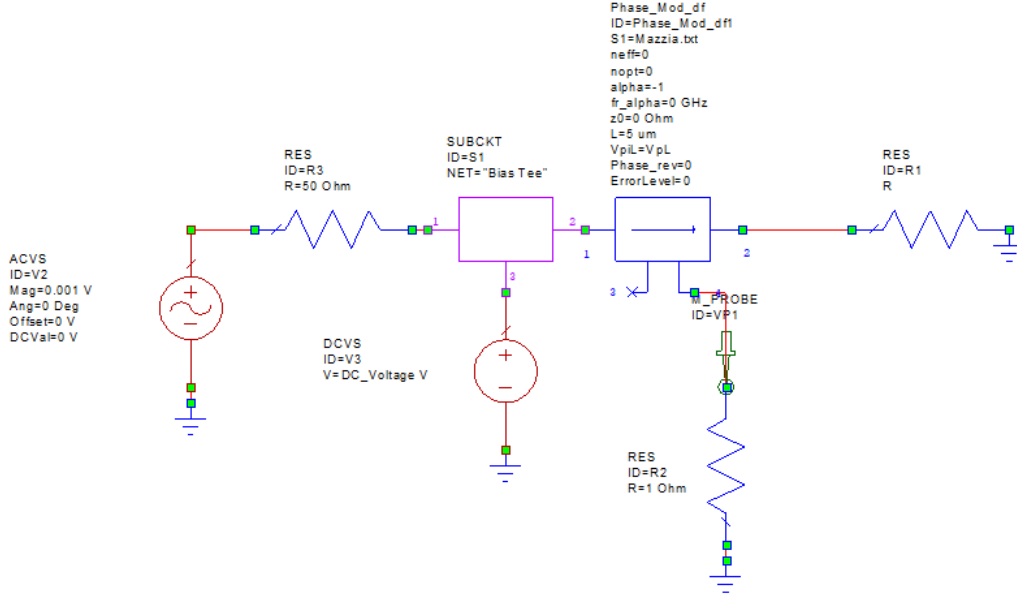


Figure 4.6. Circuit Schematic.

where

parameter	
Length L	5 μm
ON-OFF voltage V_{π}	14 V
Bias Point V_{DC}	7 V
Input Power P_{in}	1 A

As stated in Ch.2, the optical variables are represented by electrical voltages and currents, in particular the input power P_{in} and the output phase Φ_{out} correspond respectively to two currents: I_{in} (current generated by the current generator) and I_{out} (current at the output of the phase modulator block). The simulation has been conducted for a device loaded with different impedance values in order to show its behaviour in various cases.

Following, simulations in large signal condition and small signal one have been taken. Starting from the small signal simulation, in Fig. 4.8 can be seen the reference circuit, where the setting parameters are the one proposed in Fig. 4.3.

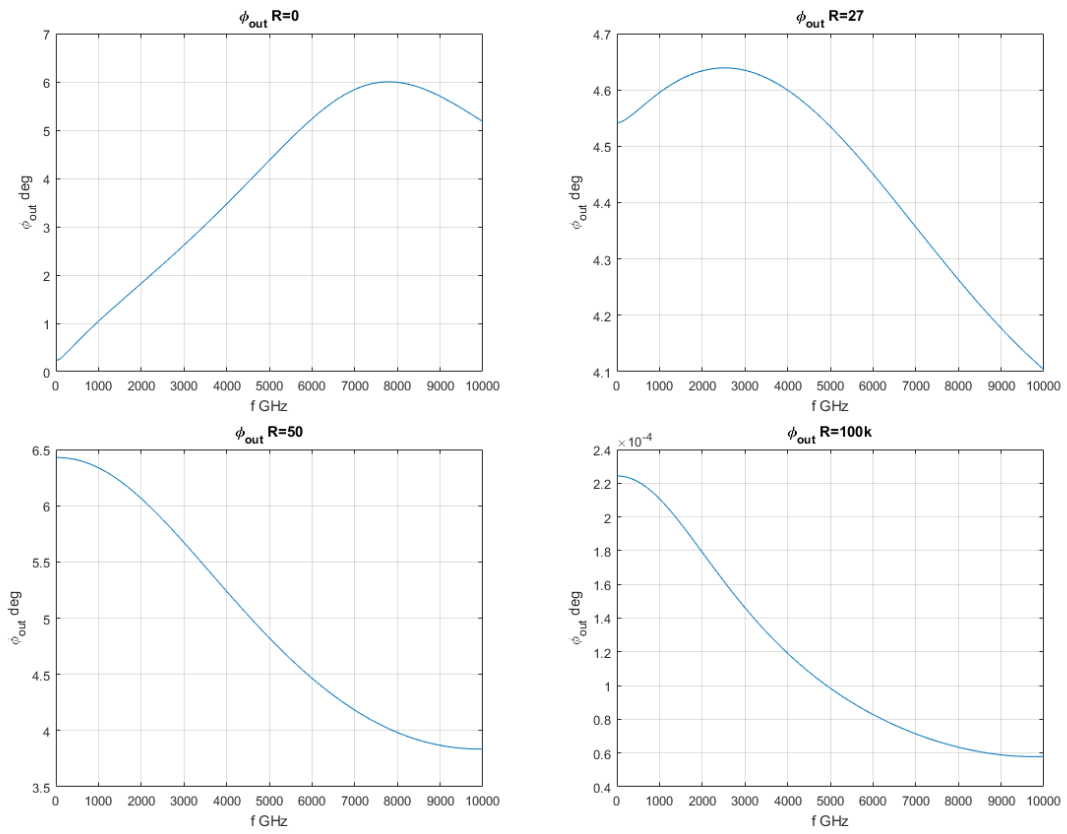


Figure 4.7. Output Phase Shift.

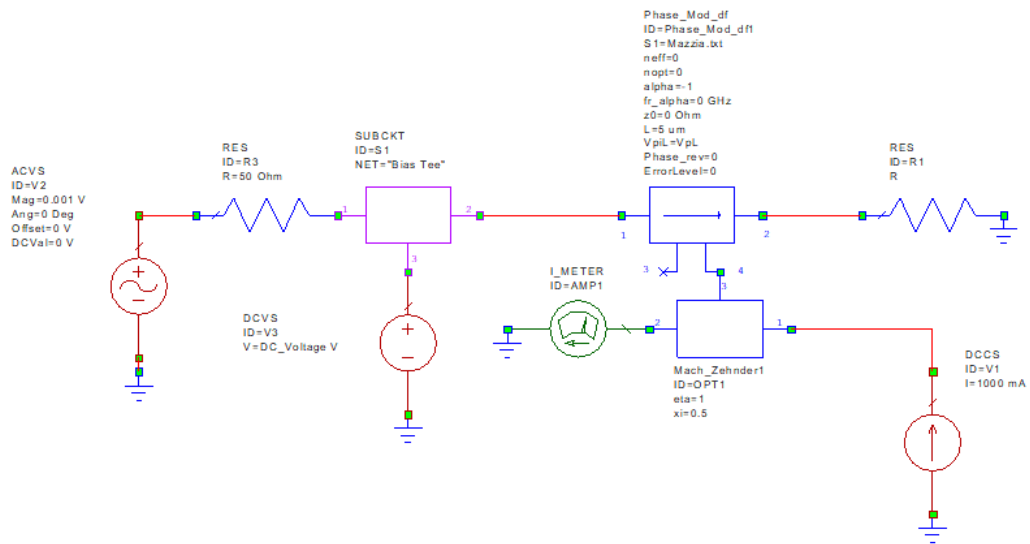


Figure 4.8. Small Signal Circuit Schematic.

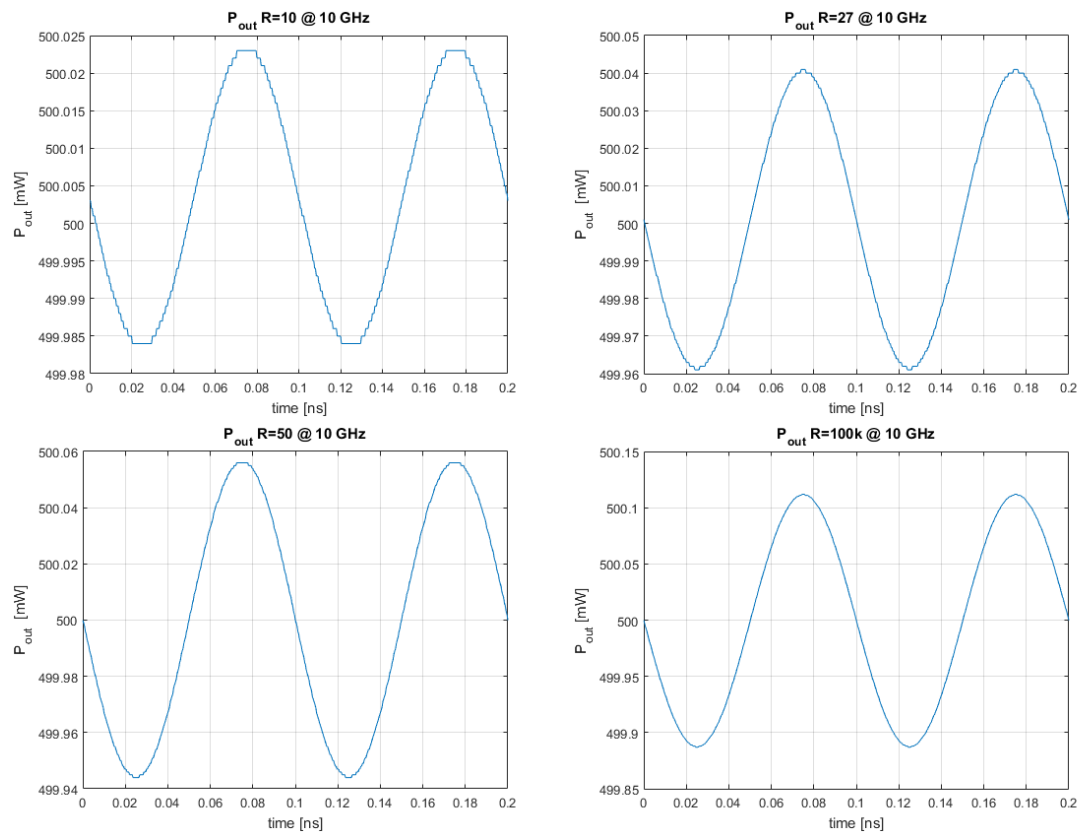


Figure 4.9. Small Signal Response.

The simulations have been performed around the bias point ($\sim V_\pi/2$) in order to be in the optimum conditions for linearity at 10GHz. The input signal is a sinusoid whose peak to peak voltage is 1mV, it is generated by a voltage generator and loaded with 50Ω impedance.

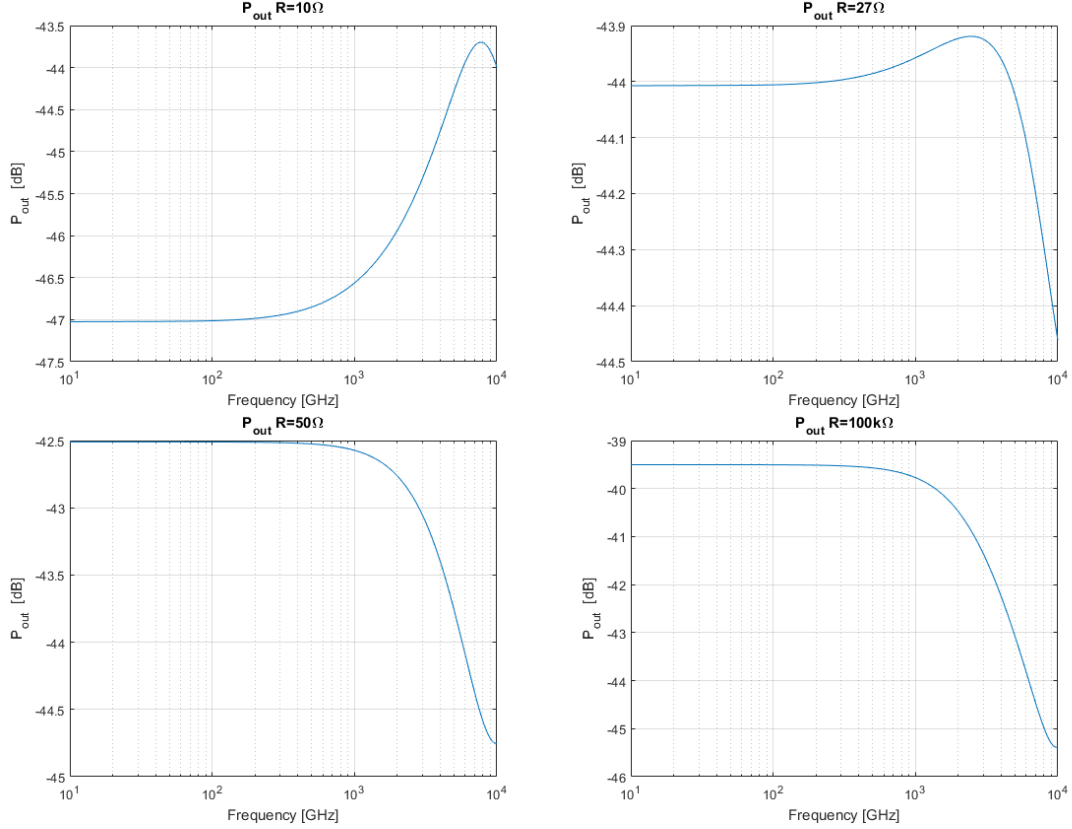


Figure 4.10. Frequency Response.

Since the parasitics have been neglected, it is possible to notice that the 3dB bandwidth is in the range of THz.

When simulating in small signal condition (and large signal one), an anomaly has been noticed: the working point is not maintained when the short circuit load is simulated with a zero resistance or value lower than 10Ω .

Finally a large signal simulation is performed in order to show how the signal is distorted. The input signal is a square wave with a peak to peak voltage $V = 14V$ (Fig.4.13). It can be noticed a variation of the excursion of the power amplitude (Fig.4.14). It is caused by a reduction of the peak to peak voltage at the input of phase block due to the resistive division between the input port impedance and the load. It will not affect significantly the overall performances since the device has shown good results even when it works not precisely in the ON or OFF states [8].

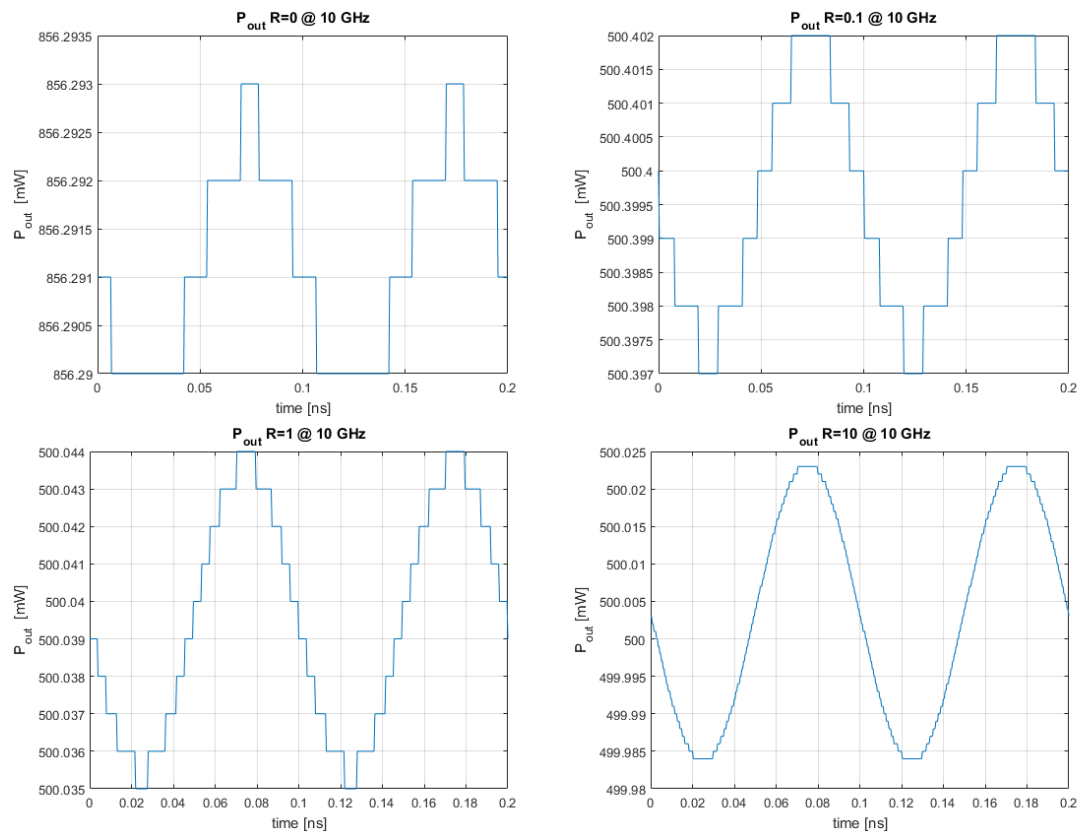


Figure 4.11. Small Signal Response:anomaly.

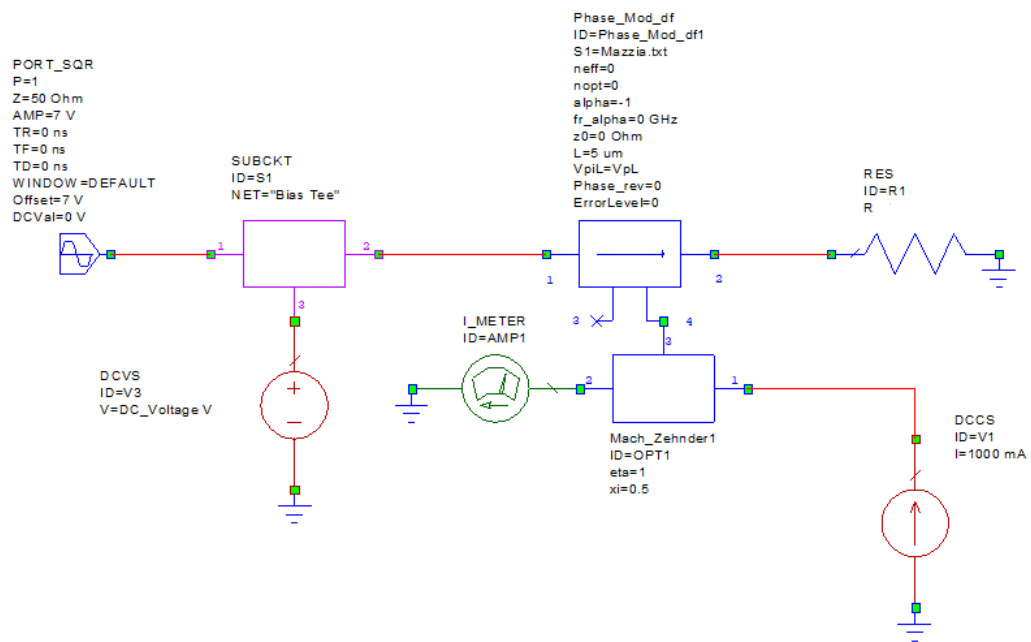


Figure 4.12. Circuit Schematic for Distortion.

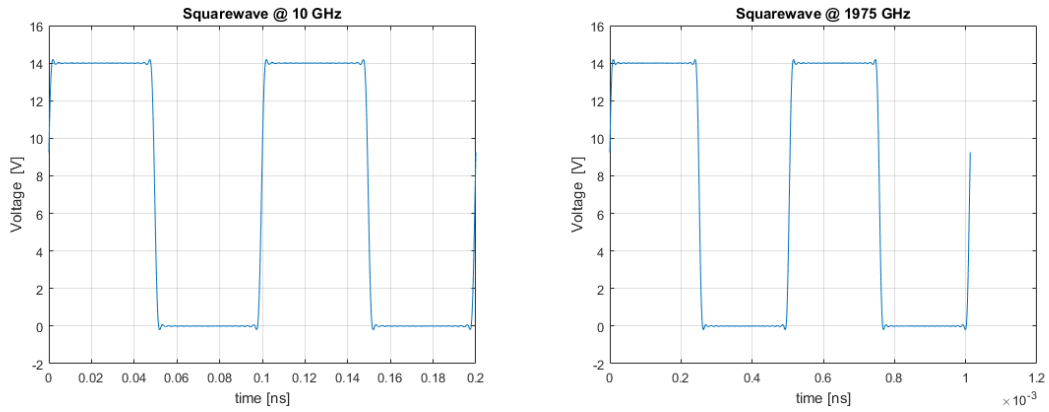


Figure 4.13. Input Signals.

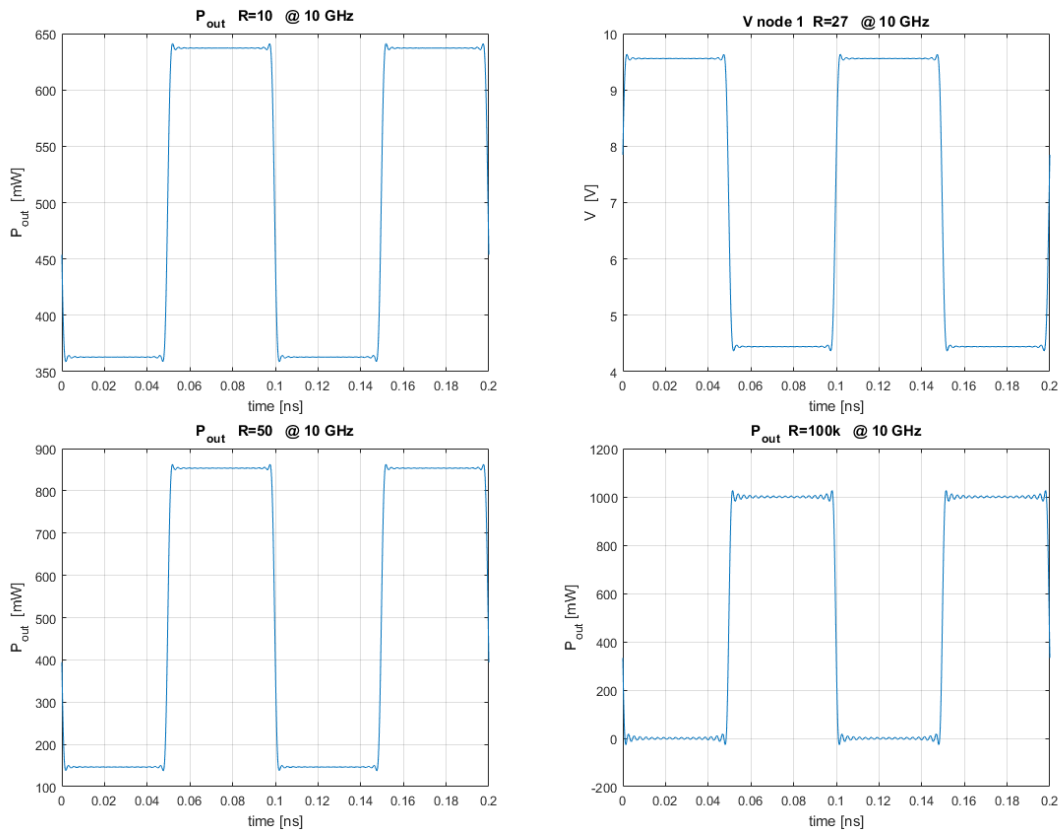


Figure 4.14. Distortion.

The presence of distortion, noticed in the large signal simulations, has a double nature, a linear one caused by the modulation itself and a nonlinear distortion due

to non-linear electro-optic response: the shape of the transfer function $T(V_{in})$ is a raised cosine.

Bibliography

- [1] G. Ghione, *Semiconductor devices for high-speed optoelectronic*. Cambridge University Press, 2009.
- [2] G. Ghione, *TCAD and system-level modelling of Mach Zehnder electro-optic modulators Draft V1.0.*
- [3] P. Zandano, *Electrical and electro-optic simulations of high-speed LiNbO₃ modulators.*
- [4] National Instruments. *Microwave Office RF Design Software*. National Instrument, 2018.
- [5] Marco Pirola, Federica Cappelluti, Giovanni Giarola and Giovanni Ghione. Multisectional Modeling of high-speed electrooptic modulators integrated in a microwave circuit CAD environment. *Journal of lightwave technology*, 21(12):2989-2996, 2003.
- [6] Sophocles J Orfanidis, Fioriti M., *Electromagnetic waves and antennas, 2016*, Unpublished, available: <http://ecweb1.rutgers.edu/orfanidi/ewa/ewa-1up.pdf>
- [7] Christian Haffner, Wolfgang Heni, Yuriy Fedoryshyn, Jens Niegemann, Argishti Melikyan, Delwin L Elder, Benedikt Baeuerle, Yannick Salamin, Arne Josten, Ueli Koch, et al. All-plasmonic Mach–Zehnder modulator enabling optical high-speed communication at the microscale. *Nature Photonics*, 9(8):525, 2015.
- [8] Wolfgang Heni, C. Haffner, Benedikt Baeuerle, Y Fedoryshyn, Arne Josten, David Hillerkuss, J Niegemann, A Melikyan, M Kohl, DL Elder, et al. Plasmonic organic hybrid modulators-scaling highest speed photonics to the microscale. *Proceedings of the IEEE*, 104(12):2362–2379, 2016.
- [9] Christian Haffner, Wolfgang Heni, Yuriy Fedoryshyn, Jens Niegemann, Argishti Melikyan, Delwin L Elder, Benedikt Baeuerle, Yannick Salamin, Arne Josten, Ueli Koch, et al. All-plasmonic Mach–Zehnder modulator enabling optical high-speed communication at the microscale - Supplementary material. *Nature Photonics*, 9(8):525, 2015.
- [10] Wolfgang Heni, C. Haffner, Benedikt Baeuerle, Y Fedoryshyn, Arne Josten, David Hillerkuss, J Niegemann, A Melikyan, M Kohl, DL Elder, et al. 108 Gbit/s plasmonic Mach–Zehnder modulator with 70-GHz electrical bandwidth. *Journal of Lightwave Technology*, 34(2):393–400, 2016.
- [11] Benedikt Baeuerle, Claudia Hoessbacher, Wolfgang Heni, Yuriy Fedoryshyn,

Arne Josten, Christian Haffner, Tatsuhiko Watanabe, Delwin L Elder, Larry R Dalton, and Juerg Leuthold. 1Driver-Less Sub 1 Vpp Operation of a Plasmonic-Organic Hybrid Modulator at 100 GBd NRZ. In *2018 Optical Fiber Communications Conference and Exposition (OFC)*, pages 1–3. IEEE, 2018.